Check for updates

Water Resources Research

RESEARCH ARTICLE
10.1029/2022WR034158

A Novel Semi-Analytical (Inertial) Solution for Determining Permeability of Highly Pervious Porous Materials Using the Two-Reservoir Laboratory Setup

Filip Stanić[1], Ognjen Govedarica[1], Nenad Jaćimović[1], Branislava Lekić[1], and Anja Ranđelović[1]

[1]Faculty of Civil Engineering, Department for Hydraulics and Environmental Engineering, University of Belgrade, Belgrade, Serbia

Key Points:

- The constant and the falling head permeability tests are not useful for highly pervious porous samples of large sizes
- A new semi-analytical model considering Forchheimer's high-velocity flow through the sample and inertia of the fluid mass is proposed here
- This formula is applied on a new permeability test where water flows through a highly pervious sample located between two reservoirs

Supporting Information:

Supporting Information may be found in the online version of this article.

Correspondence to:

F. Stanić,
fstanic@grf.bg.ac.rs;
fstanic991@gmail.com

Citation:

Stanić, F., Govedarica, O., Jaćimović, N., Lekić, B., & Ranđelović, A. (2023). A novel semi-analytical (inertial) solution for determining permeability of highly pervious porous materials using the two-reservoir laboratory setup. *Water Resources Research*, *59*, e2022WR034158. https://doi.org/10.1029/2022WR034158

Received 20 NOV 2022
Accepted 8 JUN 2023

© 2023. The Authors.
This is an open access article under the terms of the Creative Commons Attribution-NonCommercial-NoDerivs License, which permits use and distribution in any medium, provided the original work is properly cited, the use is non-commercial and no modifications or adaptations are made.

Abstract Two conventional experimental procedures for determination of the water permeability of saturated porous medium are the constant and the falling head permeability tests. The first one is more applicable on more permeable materials where the outflow from the sample is measured at variety of constant water heads, while the second one is more convenient for low permeable materials, utilizing the continuous measurements of the water head falling due to filtration through the saturated sample. However, neither of the two is useful for materials of high permeability and large cross-sectional area. The constant head permeability test faces technical issues since a significant and continuous water discharge is required, while the falling head permeability test has limitations due to neglection of the Forchheimer's high-velocity flow through the sample, but also the influence of inertia on the fluid mass. Here we proposed an approach for determination of the water permeability of saturated porous medium based on the agreement between the measured water level change in two connected reservoirs containing a porous sample and the new semi-analytical expression describing that change by accounting for the mentioned theoretical deficiencies. This efficient approach has been tested on four pervious paver samples, and results showed satisfactory agreement with the constant head permeability data. It has been also confirmed the proposed semi-analytical solution is more accurate than the falling head permeability approach in case of highly pervious materials, while for low permeable materials it reduces to the conventional approach.

1. Introduction

Saturated hydraulic conductivity K_{sat} is the basic and the most important hydraulic property of the porous medium essential for modeling and designing variety of structures and systems that are based on the interaction between water and porous media. In the field of contaminant transport and agronomy K_{sat} is used for water-solute transport and crop growth models (e.g., Clemente et al., 1994; Randelovic et al., 2016; Smith et al., 1995; Stanić et al., 2017; van Dam et al., 1997), while in hydrology it is used for different kinds of rainfall-runoff models (dos Santos et al., 2021; Sheikh et al., 2010). It is also the key parameter for designing irrigation and drainage systems, wells, infiltration fields (Ellafi et al., 2021; Islam et al., 2017; Zhuang et al., 2022), etc., but also variety of Nature Based Solutions (green roofs, biofilters, constructed wetlands, etc.) relying on the infiltration process for treating stormwater and reducing flooding in urban areas (Beach et al., 2005; Beryani et al., 2021; Bouzouidja et al., 2021; Lancheros et al., 2017; Pedescoll et al., 2009; Peng et al., 2020; Saxton & Rawls, 2006). In many of the mentioned fields the water flow can be both saturated and unsaturated, and hence is described through Richards equation (Richards, 1931) which commonly uses different mathematical functionalities between K_{sat} and soil water content or soil matric potential (Burdine, 1953; Mualem, 1976, etc.) that need to be defined.

For direct measurement of K_{sat} it is possible to apply both field and laboratory methods. Field tests (Reynolds & Elrick, 1991; Reynolds et al., 2000) are usually robust, fast, easy to perform and to replicate (Bagarello et al., 2004), and very convenient for determination of K_{sat} for natural, especially structured soils, while avoiding disturbing their macrostructure and functional relationship with surrounding soil (Bouma, 1982). On the other hand, laboratory tests are particularly important for different types of porous materials used for building constructions that interact with water. The two well established methods in engineering practice are the constant head permeability test and the falling head permeability test—Klute (1986), Dirksen (1999), Das (2002), Reynolds et al. (2002), ISO/TS 17892-11 (2004), ISO/FDIS 17312 (2005), and NEN5789 (2005), etc., where different variations of both methods can be found in literature (Diminescu et al., 2019). Standard constant head permeability test assumes

19447973, 2023, 7, Downloaded from https://agupubs.onlinelibrary.wiley.com/doi/10.1029/2022WR034158 by INASP/HINARI - SERBIA, Wiley Online Library on [28/11/2023]. See the Terms and Conditions (https://onlinelibrary.wiley.com/terms-and-conditions) on Wiley Online Library for rules of use; OA articles are governed by the applicable Creative Commons License

measuring the outflow from the porous sample under different fixed water pressure heads, where the highest ones can be imposed even by applying centrifugal force (Nimmo & Mello, 1991). Commonly, K_{sat} is determined by fitting Darcy's linear law with experimental data, while in case of highly permeable materials where high velocities occur even at small water head gradients causing deviation from linear regression, it is necessary to apply a more general Forchheimer's quadratic law (Forchheimer, 1901). Hence, besides K_{sat} it is also necessary to determine Forchheimer's coefficient β whose contribution is insignificant at small velocities in Darcy linear flow regime (Eck et al., 2012). On the other hand, the falling head permeability test assumes progressive drop of the initially imposed water head due to filtration through the porous material, where K_{sat} is determined based on the two selected values of water head and the corresponding times (Das, 2002; FprEN 12697-19:2019 E, 2019). The analytical expression describing this test assumes the pressure and gravity forces imposing the water flow through the sample are in equilibrium with the resistance force of the sample described through Darcy's linear law.

The constant head permeability test is more applicable on porous materials of higher permeability, while the falling head permeability test is more convenient for less permeable materials when the drop of water head is less rapid, and hence easier to monitor. As shown in Sandoval et al. (2017) on the example of highly pervious concrete, the falling head test underestimates K_{sat} values compared to the constant head test. Nevertheless, both tests are facing certain limitations when applied to highly permeable materials of large sizes. In the constant head test a significant water discharge needs to be maintained due to large contact area between the porous sample and the water, and hence it is recommended to recirculate the water as done in Nijp et al. (2017). Mariotte's bottle is another elegant and sophisticated method for controlling the water pressure head but is less convenient for highly permeable samples of large cross-sectional area because the bottle must be of a significant volume. On the other hand, the falling head test faces certain fundamental methodological limitations in case of highly permeable materials. First, due to high-velocity flow through the porous sample (Hassanizadeh & Grey, 1987) it is necessary to account for Forchheimer's quadratic law as done in Eck et al. (2012) for the purpose of developing an analytical solution for drainage behavior of slightly inclined highway pavements. Second, due to rapid change of water flow during the test, it is necessary to account for the inertia describing the acceleration of the fluid mass, which is ignored in the conventional approach. Also, for laboratory setups containing pipes of smaller diameters it is necessary to account for the friction force opposing the water flow.

This paper presents a new approach for determination of the water permeability of saturated porous medium from the continuous measurements of water level change in two connected reservoirs with a porous sample in between, which creates a resistance. If the porous sample is highly permeable, the two water levels approach each other through damped oscillations around the equilibrium state that are caused by the inertia of the fluid mass. To describe this phenomenon, a new semi-analytical solution considering the acceleration of the fluid mass and the high-velocity flow through the laboratory setup and the porous sample (Forchheimer's law), is proposed here. This approach has been tested on four lightweight pervious concrete pavers of 0.2 m × 0.2 m × 0.06 m and expected saturated hydraulic conductivity of approximately 0.01 m/s for porosity between 0.20 and 0.25, according to Brite/Euram Report (1994). To validate the results obtained, they are compared with the results of the constant head permeability test performed on the same paver samples by means of the specially designed modular laboratory setup. Finally, to emphasize the impact of inertia and Forchheimer's high-velocity flow in case of highly pervious materials, the presented semi-analytical solution is compared with the conventional falling head permeability approach.

2. Methodology

2.1. Derivation of a New Semi-Analytical Expression

High-velocity flow through a saturated porous medium is described by means of Forchheimer's law (Forchheimer, 1901):

$$\frac{\Delta H_{\text{imp}}}{\Delta L} = \frac{1}{K_{\text{sat}}} v_s + \beta {v_s}^2 \tag{1}$$

where $\frac{\Delta H_{\text{imp}}}{\Delta L}$ is the pressure head gradient [−] equal to the ratio between the water pressure head ΔH_{imp} [L] governing the flow through the porous sample and sample's thickness ΔL [L], v_s is the water flux through the sample [L/T], while K_{sat} and β are the saturated hydraulic conductivity [L/T] and Forchheimer coefficient [T^2/L^2],

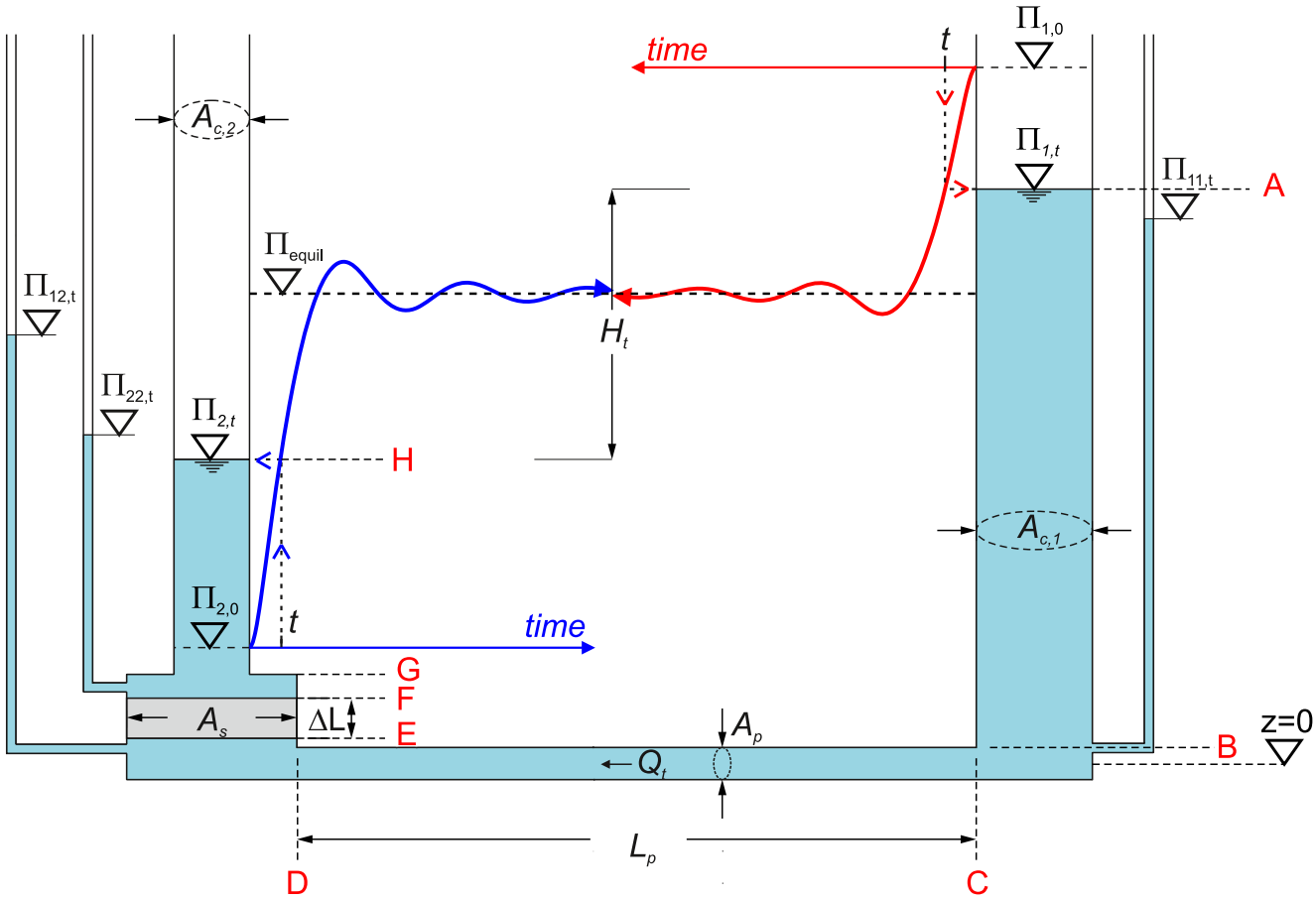

Figure 1. Schematic of the two-reservoirs test.

respectively, both describing the material's water permeability. Equation 1 shows Darcy linear behavior at small v_s, while it deviates from it as v_s increases. The boundary between dominantly linear and quadratic behavior can be roughly estimated either from the specific value of Reynolds number (order of 10) depending on the characteristic particle diameter, as suggested in some earlier studies (Bear, 1972), or based on the critical value of Forchheimer's number as proposed in Zeng and Grigg (2006).

To experimentally determine values of K_f and β for highly permeable materials of large cross-sectional area, the timesaving two-reservoir test is conducted. Figure 1 illustrates the two-reservoir laboratory setup where water flows from Reservoir 1 (cross-sectional areas $A_{c,1}$ [L^2]) on the right-hand side to Reservoir 2 (cross-sectional areas $A_{c,2}$ [L^2]) on the left-hand side, while passing first through the pipe of length L_p [L] and cross-sectional area A_p [L^2], and then through the porous sample of thickness ΔL [L] and cross-sectional area A_s [L^2]. Two water levels $\Pi_{1,t}$ and $\Pi_{2,t}$ are met at the equilibrium state Π_{equil} after damped oscillations (see Figure 1) driven by the conservation of the momentum, where the amplitude of oscillations depend on the resistance force opposing the flow.

This phenomenon can be described by means of two equations: the water balance equation and the momentum equation. The first one defines water flow Q_t [L^3/T] as the change of $\Pi_{1,t}$ and $\Pi_{2,t}$ in time:

$$Q_t = -\frac{d\Pi_{1,t}}{dt} A_{c,1} = \frac{d\Pi_{2,t}}{dt} A_{c,2} \tag{2}$$

where index t describes variation in time. Due to oscillations of water levels, Q_t changes the sign depending on the flow direction, where Q_t is positive when $\Pi_{1,t}$ decreases and $\Pi_{2,t}$ rises, while otherwise it is negative. Since $H_t = \Pi_{1,t} - \Pi_{2,t}$ (see Figure 1), Q_t can be expressed from Equation 2 as following:

$$Q_t = -\frac{dH_t}{dt} A_e \tag{3}$$

19447973, 2023, 7, Downloaded from https://agupubs.onlinelibrary.wiley.com/doi/10.1029/2022WR034158 by INASP/HINARI - SERBIA, Wiley Online Library on [28/11/2023]. See the Terms and Conditions (https://onlinelibrary.wiley.com/terms-and-conditions) on Wiley Online Library for rules of use; OA articles are governed by the applicable Creative Commons License

$$A_e = \frac{A_{c,1}A_{c,2}}{A_{c,1} + A_{c,2}} \tag{4}$$

where A_e is the equivalent cross-sectional area [L^2].

The momentum equation relies on Newton's Second Law defining the change in momentum per change in time (mass multiplied with acceleration = velocity change in time) as a difference between the driving force (water pressure and gravity) governing the flow and the resistance force opposing the flow. Since force is a vector, to avoid summing up vectors along the complex flow path, it is convenient to divide the laboratory setup from Figure 1 into sections of constant direction and geometry, and then to deal only with vector intensities (scalars). Hence, the momentum equation in scalar form is written between consecutive sections A-B, C-D, E-F, and G-H (see Figure 1), respectively:

$$\rho_w g A_{c1}(\Pi_{1,t} - \Pi_{11,t}) - \rho_w g A_{c1}\Delta H_{11,t} = m_{w,c1}\frac{dv_{c1,t}}{dt} \tag{5a}$$

$$\rho_w g A_p(\Pi_{11,t} - \Pi_{12,t}) - \rho_w g A_p \Delta H_{1,t} = m_{w,p}\frac{dv_{p,t}}{dt} \tag{5b}$$

$$\rho_w g A_s(\Pi_{12,t} - \Pi_{22,t}) - \rho_w g A_s \Delta H_{2,t} = m_{w,s}\frac{dv_{s,t}}{dt} \tag{5c}$$

$$\rho_w g A_{c2}(\Pi_{22,t} - \Pi_{2,t}) - \rho_w g A_{c2}\Delta H_{22,t} = m_{w,c2}\frac{dv_{c2,t}}{dt} \tag{5d}$$

In Equations 5a–5d the first term on the left-hand side represents the water pressure and gravity force (driving force) defined through the water level differences [L] at section ends, where $\Pi_{11,t}$ and $\Pi_{22,t}$ are the water heads [L] at the bottom of Reservoirs 1 and 2, respectively, while $\Pi_{12,t}$ is the water head [L] just below the sample. The second term in Equations 5a–5d is the resistance force opposing the flow, where $\Delta H_{1,t}$, $\Delta H_{11,t}$ and $\Delta H_{22,t}$ are the energy losses in length units [L] due to friction along the pipe and Reservoirs 1 and 2, respectively, while $\Delta H_{2,t}$ is the energy loss [L] due to impedance of the porous sample. Finally, the right-hand side in all four equations describes the change in momentum per change in time, where $m_{w,c1}$ and $m_{w,c2}$ are the fluid masses in Reservoirs 1 and 2, respectively, $m_{w,p}$ and $m_{w,s}$ are the fluid masses in the pipe and in the sample, respectively, while $v_{c1,t}$ [L/T], $v_{c2,t}$ [L/T] and $v_{p,t}$ [L/T] are the water fluxes in the corresponding sections ($v_{s,t}$ is as in Equation 1, ρ_w is water density [M/L^3] and g is the acceleration of gravity [L/T^2]). After substituting $m_{w,c1} = \rho_w A_{c1}\Pi_{1,t}$, $m_{w,c2} = \rho_w A_{c2}(\Pi_{2,t} - \Delta L)$, $m_{w,p} = \rho_w A_p L_p$ and $m_{w,s} = n\rho_w A_s \Delta L$, where n is sample porosity [−], into Equations 5a–5d, together with $v_{c1,t} = \frac{Q_t}{A_{c1}}$, $v_{c2,t} = \frac{Q_t}{A_{c2}}$, $v_{p,t} = \frac{Q_t}{A_p}$, and $v_{s,t} = \frac{Q_t}{A_s}$, the following is obtained:

$$(\Pi_{1,t} - \Pi_{11,t}) - \Delta H_{11,t} = \frac{\Pi_{1,t}}{gA_{c1}}\frac{dQ_t}{dt} \tag{6a}$$

$$(\Pi_{11,t} - \Pi_{12,t}) - \Delta H_{1,t} = \frac{L_p}{gA_p}\frac{dQ_t}{dt} \tag{6b}$$

$$(\Pi_{12,t} - \Pi_{22,t}) - \Delta H_{2,t} = \frac{n\Delta L}{gA_s}\frac{dQ_t}{dt} \tag{6c}$$

$$(\Pi_{22,t} - \Pi_{2,t}) - \Delta H_{22,t} = \frac{\Pi_{2,t} - \Delta L}{gA_{c2}}\frac{dQ_t}{dt} \tag{6d}$$

By summing Equations 6a–6d, the following is obtained:

$$H_t - \left(\Delta H_{f,t} + \Delta H_{\mathrm{imp},t}\right) = I_t \tag{7}$$

where $\Delta H_{f,t} = \Delta H_{1,t} + \Delta H_{11,t} + \Delta H_{22,t}$, $\Delta H_{imp,t} = \Delta H_{2,t}$ is like in Equation 1, while $I_t = c_t\frac{dQ_t}{dt}$ and $c_t = \frac{\Pi_{1,t}}{gA_{c1}} + \frac{\Pi_{2,t}-\Delta L}{gA_{c2}} + \frac{L_p}{gA_p} + \frac{n\Delta L}{gA_s}$. Note that c_t is a function of time when $A_{c1} \neq A_{c2}$, while its value is constant for $A_{c1} = A_{c2}$ due to conservation of the fluid length in Reservoirs 1 and 2 ($\Pi_{1,t} + \Pi_{2,t}$ = const). The case where

19447973, 2023, 7, Downloaded from https://agupubs.onlinelibrary.wiley.com/doi/10.1029/2022WR034158 by INASP/HINARI - SERBIA, Wiley Online Library on [28/11/2023]. See the Terms and Conditions (https://onlinelibrary.wiley.com/terms-and-conditions) on Wiley Online Library for rules of use; OA articles are governed by the applicable Creative Commons License

$A_{c1} = A_{c2} = A_p = A_s$ relates to the laboratory setup with uniform cross-sectional area (something similar to the U-shaped pipe), while in case of large Reservoirs 1 and 2 ($A_{c1} \gg A_p$ and $A_{c2} \gg A_p$) c_t reduces to the constant value $c = \frac{L_p}{gA_p} + \frac{n\Delta L}{gA_s}$, or even to $c = \frac{L_p}{gA_p}$ for samples of small thickness where $\frac{L_p}{gA_p} \gg \frac{n\Delta L}{gA_s}$. Also, when $A_{c1} \gg A_p$ and $A_{c2} \gg A_p$, which is usually the case, energy losses in vertical columns $\Delta H_{11,t}$ and $\Delta H_{22,t}$ are negligible, and hence $\Delta H_{f,t} = \Delta H_{1,t}$.

Equation 7 is expressed in length units [L], where H_t represents the driving force (gravity and pressure), I_t is the inertial force [L] describing the acceleration of the fluid mass, while ($\Delta H_{f,t} + \Delta H_{\text{imp},t}$) represents the total resistance force which consists of the friction ($\Delta H_{f,t}$) and the impedance of the porous material ($\Delta H_{\text{imp},t}$). The friction and the impedance components can be expressed as a function of Q_t:

$$\Delta H_{f,t} = r_Q Q_t |Q_t| \tag{8}$$

$$\Delta H_{\text{imp},t} = aQ_t + bQ_t|Q_t| \tag{9}$$

Note that $Q_t|Q_t|$ is used instead of ${Q_t}^2$ in both Equations 8 and 9 to account for the change of flow direction. $\Delta H_{f,t}$ is described by means of a friction factor r_Q [T^2/L^5] which depends on Q_t and is determined from Darcy-Weisbach equation (Nakayama & Boucher, 1998) as explained in Appendix A, while $\Delta H_{\text{imp},t}$ is expressed from Forchheimer's law (Equation 1) by substituting $v_{s,t} = \frac{Q_t}{A_s}$ and by using coefficients a and b that are equal to:

$$a = \frac{\Delta L}{K_{\text{sat}} A_s} \tag{10}$$

$$b = \frac{\beta \Delta L}{{A_s}^2} \tag{11}$$

After introducing Equations 8 and 9 into Equation 7, and substituting Q_t with Equation 3, the following is obtained:

$$-c_t A_e \frac{d^2 H_t}{dt^2} - aA_e \frac{dH_t}{dt} - (r_Q + b){A_e}^2 \frac{dH_t}{dt}\left|\frac{dH_t}{dt}\right| - H_t = 0 \tag{12}$$

The presented nonlinear Ordinary Differential Equation 12 of the second order has no continuous analytical solution over time and must be solved numerically as presented in Appendix B. However, if considering a short time interval Δt where Q_t is strictly positive, it is reasonable to assume a constant driving force H_t, as well as c_t and r_Q. Hence, Equation 12 is transformed using Equation 3 to express Q_t:

$$c_t \frac{dQ_t}{dt} + aQ_t + (r_Q + b){Q_t}^2 - H_{t-\Delta t} = 0 \tag{13}$$

To have the constant pressure and gravity component in Equation 13, the value from the previous time interval $H_{t-\Delta t}$ is used. Equation 13 is first solved with respect to Q_t by rearranging it and separating variables:

$$\frac{dQ_t}{aQ_t + (r_Q + b){Q_t}^2 - H_{t-\Delta t}} = -\frac{dt}{c_t} \tag{14}$$

$$\frac{dQ_t}{\left(Q_t\sqrt{(r_Q+b)} + \frac{a}{2\sqrt{(r_Q+b)}}\right)^2 - \left(\frac{a^2}{4(r_Q+b)} + H_{t-\Delta t}\right)} = -\frac{dt}{c_t} \tag{15}$$

Before integrating Equation 15 the following substitutions are introduced:

$$X = Q_t\sqrt{(r_Q+b)} + \frac{a}{2\sqrt{(r_Q+b)}} \tag{16}$$

$$S = \sqrt{\frac{a^2}{4(r_Q+b)} + H_{t-\Delta t}} \tag{17}$$

19447973, 2023, 7, Downloaded from https://agupubs.onlinelibrary.wiley.com/doi/10.1029/2022WR034158 by INASP/HINARI - SERBIA, Wiley Online Library on [28/11/2023]. See the Terms and Conditions (https://onlinelibrary.wiley.com/terms-and-conditions) on Wiley Online Library for rules of use; OA articles are governed by the applicable Creative Commons License

19447973, 2023, 7, Downloaded from https://agupubs.onlinelibrary.wiley.com/doi/10.1029/2022WR034158 by INASP/HINARI - SERBIA, Wiley Online Library on [28/11/2023]. See the Terms and Conditions (https://onlinelibrary.wiley.com/terms-and-conditions) on Wiley Online Library for rules of use; OA articles are governed by the applicable Creative Commons License

Where based on Equation 16 $dQ_t = \frac{dX}{\sqrt{(r_Q+b)}}$. Hence, Equation 15 becomes as following:

$$\frac{1}{\sqrt{(r_Q+b)}}\int \frac{dX}{X^2-S^2} = -\int \frac{dt}{c_t} \tag{18}$$

By solving integrals on the left-hand and the right-hand side of Equation 18, the following is obtained:

$$-\frac{1}{S\sqrt{(r_Q+b)}}\tanh^{-1}\left(\frac{X}{S}\right) = -\frac{t}{c_t} + G \tag{19}$$

where G is the integration constant defined later. By introducing Equation 16 into Equation 19, an expression describing Q_t is obtained:

$$Q_t = \frac{S}{\sqrt{(r_Q+b)}}\tanh\left(S\sqrt{(r_Q+b)}\left(\frac{t}{c_t}-G\right)\right) - \frac{a}{2(r_Q+b)} \tag{20}$$

To preserve the continuity of Equation 20 in time, Q_t at $t-\Delta t$ should be equal to $Q_{t-\Delta t}$ from the previous time step. Hence, G can be easily determined from Equation 20 as:

$$G = \frac{t-\Delta t}{c_t} - \frac{1}{S\sqrt{(r_Q+b)}}\tanh^{-1}\left(\frac{\sqrt{(r_Q+b)}}{S}\left(Q_{t-\Delta t}+\frac{a}{2(r_Q+b)}\right)\right) \tag{21}$$

To derive the expression for H_t, Equation 3 is introduced back into Equation 21 and variables are separated:

$$\int_{H_{t-\Delta t}}^{H_t} dH_t = -\int_{t-\Delta t}^{t}\left(\frac{S}{A_e\sqrt{(r_Q+b)}}\tanh\left(S\sqrt{(r_Q+b)}\left(\frac{t}{c_t}-G\right)\right) - \frac{a}{2A_e(r_Q+b)}\right)dt \tag{22}$$

By integrating the left-hand side from $H_{t-\Delta t}$ to H_t and the right-hand side from $t-\Delta t$ to t, the following is obtained:

$$H_t - H_{t-\Delta t} = \frac{a}{2A_e(r_Q+b)}t\Big|_{t-\Delta t}^{t} - \frac{c_t}{S\sqrt{(r_Q+b)}}\frac{S}{A_e\sqrt{(r_Q+b)}}\ln\left(\cosh\left(S\sqrt{(r_Q+b)}\left(G-\frac{t}{c_t}\right)\right)\right)\Big|_{t-\Delta t}^{t} \tag{23}$$

Finally, H_t can be expressed from Equation 23 as below:

$$H_t = H_{t-\Delta t} + \frac{a\Delta t}{2A_e(r_Q+b)} - \frac{c_t}{A_e(r_Q+b)}\ln\left(\frac{\cosh\left(S\sqrt{(r_Q+b)}\left(G-\frac{t}{c_t}\right)\right)}{\cosh\left(S\sqrt{(r_Q+b)}\left(G-\frac{t-\Delta t}{c_t}\right)\right)}\right) \tag{24}$$

By combining Equations 2 and 3 for both reservoirs, and writing them in a discrete form as $(\Pi_{1,0}-\Pi_{1,t})A_{c,1} = (H_0-H_t)A_e$ and $(\Pi_{2,t}-\Pi_{2,0})\mathrm{A}_{c,2} = (H_0-H_t)A_e$, water levels $\Pi_{1,t}$ and $\Pi_{2,t}$ are determined as:

$$\Pi_{1,t} = \Pi_{1,0} - (H_0-H_t)\frac{A_e}{A_{c,1}} \tag{25}$$

$$\Pi_{2,t} = \Pi_{2,0} + (H_0-H_t)\frac{A_e}{A_{c,2}} \tag{26}$$

where $\Pi_{1,0}$ and $\Pi_{2,0}$ are the initial water levels in Reservoirs 1 and 2 (see Figure 1), while $H_0 = \Pi_{1,0} - \Pi_{2,0}$. Once Q_t and H_t are mathematically defined through Equations 20 and 24, it is possible to determine values for each of the components in Equation 7. Hence, the friction force $\Delta H_{f,t}$ is determined from Equations 8 and 20, the impedance force $\Delta H_{\mathrm{imp},t}$ from Equations 9 and 20, while the inertial force I_t is calculated from the first derivative of Equation 20:

$$I_t = c_t \frac{dQ_t}{dt} = \left(\frac{S}{\cosh\left(S\sqrt{(r_Q + b)}\left(\frac{t}{c_t} - G \right) \right)} \right)^2 \tag{27}$$

The proposed solution is interval-based because both H_t and Q_t (and other components of Equation 7) are valid only over Δt. To obtain the continuous solution over entire time scale, the calculation is performed consecutively at each Δt relying on the values $H_{t-\Delta t}$ and $Q_{t-\Delta t}$ from the previous interval. Detailed calculation steps, including how to consider not only positive but also negative Q_t, are explained in the following section.

2.2. Calculation Steps

Water permeability parameters of a porous medium K_f and β are determined based on the best agreement between the semi-analytical H_t function (Equation 24) and the experimental H_i data. To compute H_t it is necessary to define initial conditions ($H_{t=0} = H_0$ and $Q_{t=0} = Q_0$) and values of the parameters excluded from the calibration ($A_{c,1}$, $A_{c,2}$, A_p, L_p, ΔL, A_s). H_t is then computed at each Δt using the following iterative algorithm:

1. First iteration assumes $H_t = H_{t-\Delta t}$ and $Q_t = Q_{t-\Delta t}$.
2. r_Q is computed from Equation A1.4 using the value of Q_t.
3. S is computed from Equation 17 using the value of H_t, while for $A_{c,1} \neq A_{c,2}$ value of c_t is computed using values $\Pi_{1,t}$ and $\Pi_{2,t}$ (Equations 25 and 26) obtained from H_t.
4. G is calculated by means of Equation 21 using r_Q from step 2.
5. New values of H_t and Q_t are calculated by means of Equations 24 and 20, respectively.
6. Values from step 5 are introduced back into steps 2 and 3 and the whole procedure is iteratively repeated until the absolute difference between H_t values in two consecutive iterations is less than 1×10^{-6} m.

The presented semi-analytical solution (Equation 24) assumes strictly positive Q_t, and to account for negative Q_t it is sufficient to change the sign of the term $(r_Q + b)$ which multiplies Q_t^2. Hence, $-(r_Q + b)$ is used for negative Q_t and $(r_Q + b)$ for positive Q_t. However, utilization of longer time intervals (Δt) increases the risk of missing the time when Q_t changes the sign (flow changes direction), and hence the solution might not converge. In that case convergence is obtained by temporarily reducing Δt (e.g., multiplied consecutively by factor 0.9). Even though stable, the calculation performed with rather large Δt leads to inaccurate model outcomes (H_t and Q_t) with mitigated and postponed amplitudes (see Appendix C). To prevent this, it is recommended to use $\Delta t = T/100$, where $T = 2\pi\sqrt{\frac{L_p A_e}{g A_p}}$ is the period for undamped oscillations (Ivetić, 1996) which depends solely on the installation geometry. As shown in Appendix C, this criterion for Δt selection provides both accurate and stable results regardless of material's permeability.

The quality of the fitting between the simulated H_t data and the experimental H_i data is described by means of the coefficient of determination R-squared:

$$R^2 = 1 - \frac{\sum_{i=1}^{N} (H_i - H_{ti})^2}{\sum_{i=1}^{N} \left(H_i - \overline{H_i} \right)^2} \tag{28}$$

where N is the number of experimental data [−], H_{ti} and H_i are the simulated and measured values, respectively, related to same time t_i, while $\overline{H_i}$ is the mean value of all measurements. Another measure of the fitting quality used in this work is the root mean square error (RMSE):

$$\mathrm{RMSE} = \sqrt{\frac{\sum_{i=1}^{N} (H_i - H_{ti})^2}{N}} \tag{29}$$

The closer R^2 is to unity, or the closer RMSE is to zero, the better fitting between simulated and measured data is obtained. One of the main advantages of the presented approach is its simple application which, as in case of

19447973, 2023, 7, Downloaded from https://agupubs.onlinelibrary.wiley.com/doi/10.1029/2022WR034158 by INASP/HINARI - SERBIA, Wiley Online Library on [28/11/2023]. See the Terms and Conditions (https://onlinelibrary.wiley.com/terms-and-conditions) on Wiley Online Library for rules of use; OA articles are governed by the applicable Creative Commons License

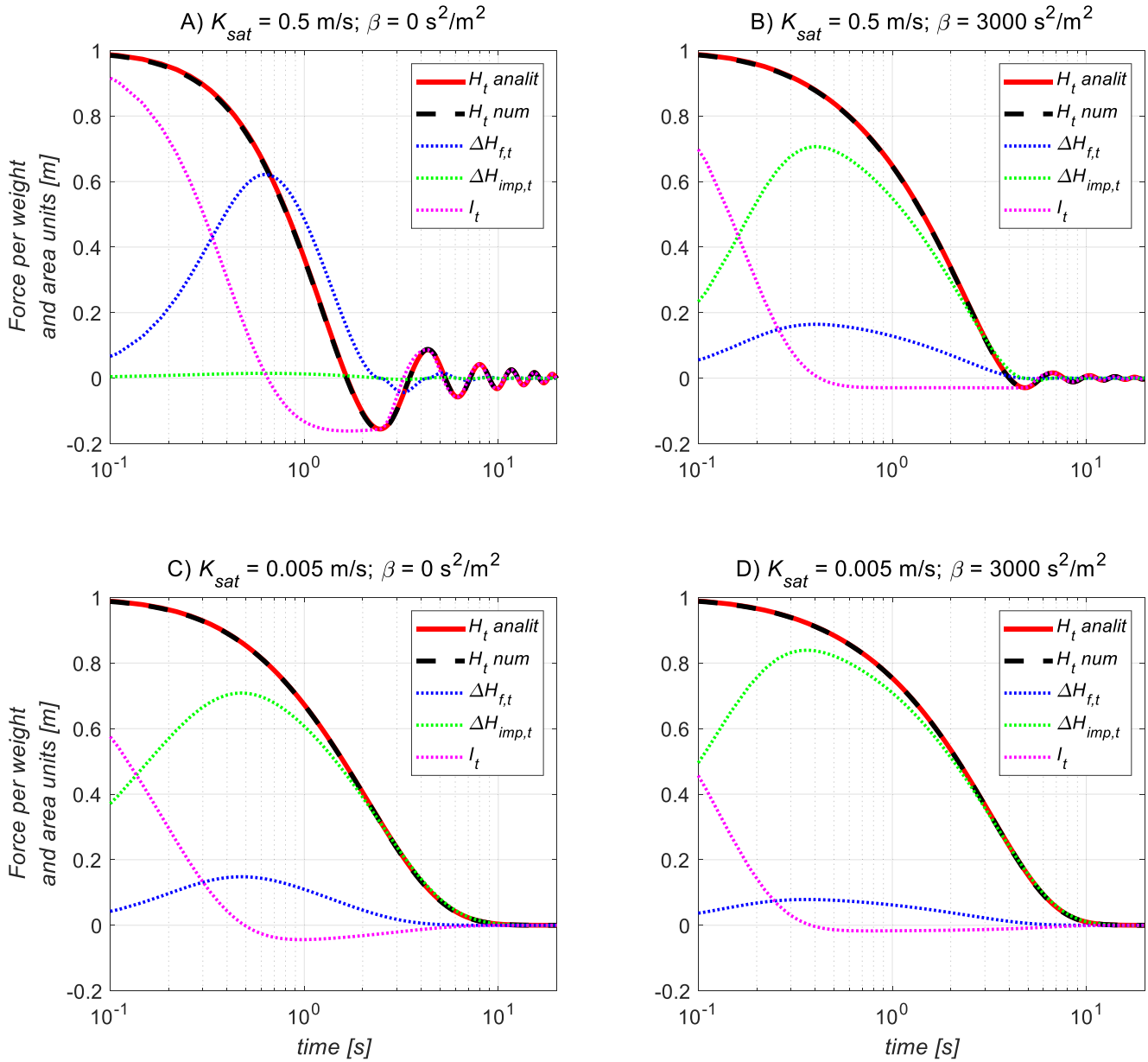

Figure 2. Comparison between the proposed semi-analytical approach (Equation 24—red solid line) and the numerical model (Equation B1.3—black dashed line) for different combinations of K_{sat} and β values, and pipe **ϕ50.8 mm**; H_0 = 1 m, Q_0 = 0 L/s, ΔL = 0.06 m, A_s = 0.04 m^2, $\boldsymbol{A_p = 2 \times 10^{-3}}$ **m^2 (ϕ50.8 mm),** L_p = 1.1 m, and $A_{c,1} = A_{c,2}$ = 0.0123 m^2 (ϕ125 mm).

the falling head permeability test, only requires continuous measurements of water levels in two reservoirs, $\Pi_{1,i}$ and $\Pi_{2,i}$ ($H_i = \Pi_{1,i} - \Pi_{2,i}$).

2.3. Impact of Parameters K_f and β

The accuracy of the proposed approach is validated through the comparison with the numerical model for solving Equation 12 (see Appendix B). Figure 2 illustrates the comparison between Equation 24 (red solid line) and the numerical model (black dashed line) for different combinations of K_{sat} and β values. Figure 3 presents similar comparison but using smaller pipe diameter D_p = 25.4 mm to show strong dependence of the friction force on the pipe diameter, but also its effect on the sensitivity of Equation 24 to K_{sat} and β.

19447973, 2023, 7, Downloaded from https://agupubs.onlinelibrary.wiley.com/doi/10.1029/2022WR034158 by INASP/HINARI - SERBIA, Wiley Online Library on [28/11/2023]. See the Terms and Conditions (https://onlinelibrary.wiley.com/terms-and-conditions) on Wiley Online Library for rules of use; OA articles are governed by the applicable Creative Commons License

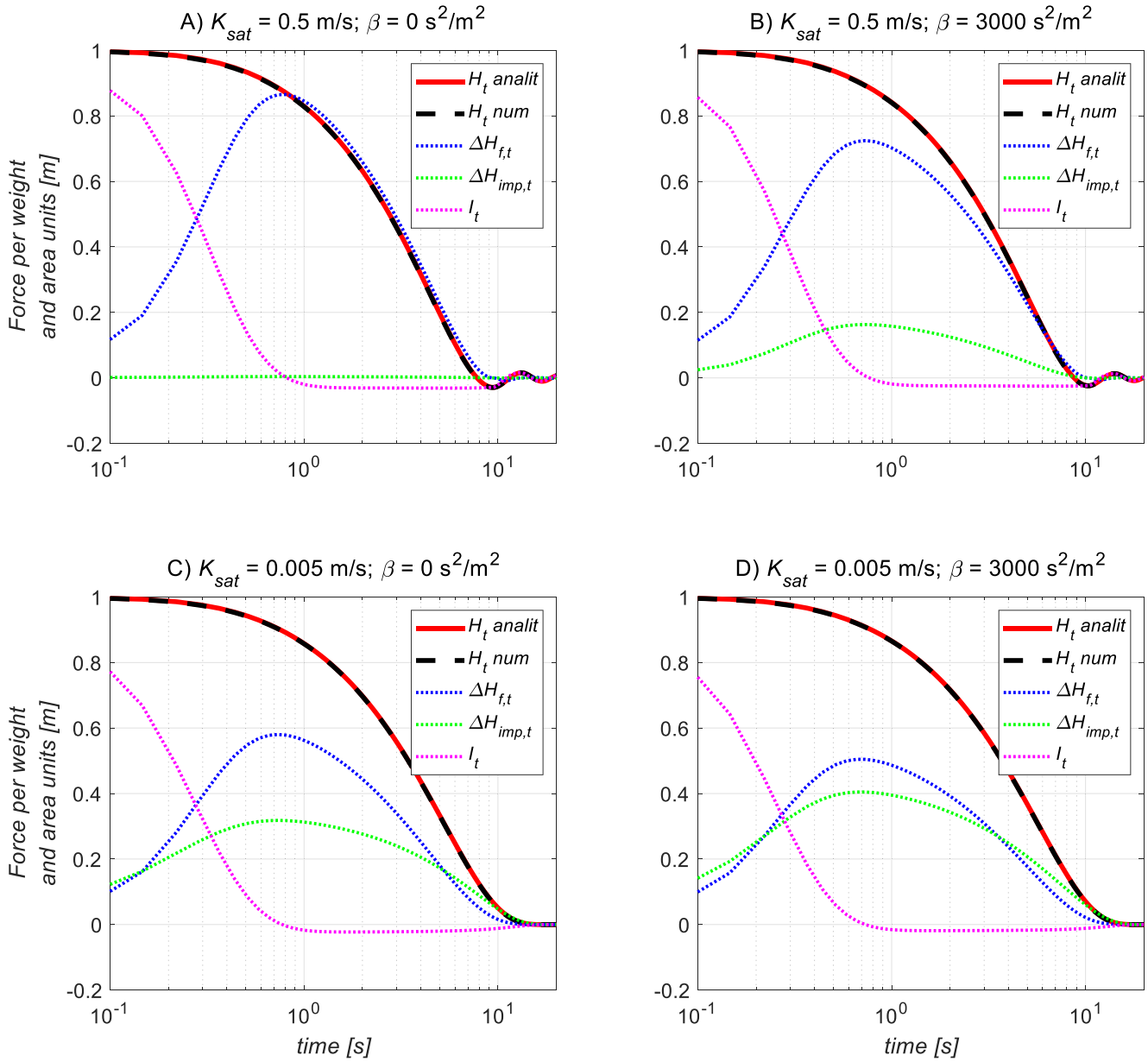

Figure 3. Comparison between the proposed semi-analytical approach (Equation 24—red solid line) and the numerical model (Equation B1.3—black dashed line) for different combinations of K_{sat} and β values, and pipe $\boldsymbol{D_p = 25.4\ mm}$; $H_0 = 1$ m, $Q_0 = 0$ L/s, $\Delta L = 0.06$ m, $A_s = 0.04$ m^2, $\boldsymbol{A_p = 5 \times 10^{-4}\ m^2}$ **(ϕ25.4 mm),** $L_p = 1.1$ m, and $A_{c,1} = A_{c,2} = 0.0123$ m^2 (ϕ125 mm).

In case of Figure 2, a larger pipe diameter is responsible for less significant friction force $\Delta H_{f,t}$ (dotted blue line) giving more weight to the impedance force $\Delta H_{\text{imp},t}$ (dotted green line). Only in Figure 2a where the water permeability of a porous medium is the most significant, and hence Q_t is the highest, $\Delta H_{f,t}$ is dominant over $\Delta H_{\text{imp},t}$, while in other cases its impact is much lower. Figure 2a shows how considerable oscillations of H_t occur when there is no strong resistance force opposing the pressure and gravity, which is manifested with significant I_t (dotted magenta line). As the water permeability decreases (K_{sat} decreases or β increases, Figures 2b–2d) the total resistance force increases, where $\Delta H_{\text{imp},t}$ becomes dominant over $\Delta H_{f,t}$ due to reduced Q_t. Hence, I_t is mitigated and oscillations of H_t are damped. This confirms that for low permeable materials, when both the friction and the inertia are negligible, the proposed semi-analytical solution reduces to the standard "quasi-steady state" approach accounting only for the impedance force opposing the pressure and gravity force.

19447973, 2023, 7, Downloaded from https://agupubs.onlinelibrary.wiley.com/doi/10.1029/2022WR034158 by INASP/HINARI - SERBIA, Wiley Online Library on [28/11/2023]. See the Terms and Conditions (https://onlinelibrary.wiley.com/terms-and-conditions) on Wiley Online Library for rules of use; OA articles are governed by the applicable Creative Commons License

On the other hand, when using two times smaller pipe diameter as in Figure 3, $\Delta H_{f,t}$ remains important regardless of K_{sat} and β values. As shown in Figure 3a for the same K_{sat} and β values, oscillations of H_t are significantly lower compared to Figure 2a. Since $\Delta H_{f,t}$ contributes highly to the total resistance force, H_t is less sensitive to K_{sat} and β than in Figure 2 where $\Delta H_{imp,t}$ is dominant. This might be an issue when estimating value of β (or b) because both r_Q and b are related to Q_t^2 (see Equations 8 and 9), so r_Q when significant conceals the impact of b. Therefore, to increase the accuracy of the proposed semi-analytical solution in estimation of K_{sat} and β values, it is recommended to reduce the impact of pipe friction as much as possible. Ideally, the pipe diameter like that of the two reservoirs is to be used, transforming that way the laboratory setup into the U-shaped pipe. Since this is not always technically feasible, it is highly recommended to run the simulation with the assumed values of K_{sat} and β and various pipe dimensions to find the adequate D_p and L_p that secure $\Delta H_{f,t}$ inferior to $\Delta H_{imp,t}$.

The proposed solution provides almost identical results as the numerical model for various combinations of K_{sat} and β. Both models are efficient, and the typical computation time is about 0.1 s for 20 s long simulation period and rather small $\Delta t = 0.01$ s. However, the advantage of the proposed semi-analytical model over the numerical one, besides its simpler application and better accuracy due to its analytical nature, is its capability to use twice as large Δt when most significant and rapid H_t oscillations occur (as in Figure 2a).

3. Laboratory Setup and Samples

Figure 4 illustrates the modular laboratory setup specially designed to cope with the two-reservoirs test proposed here, but also with the standard constant head permeability test which is used as a reference in this study. Both tests, together with detailed instructions for performing them, are thoroughly explained in the following text.

3.1. Constant Head Permeability Test

The constant head permeability test requires plenty of water, which is why the laboratory setup presented in Figure 4 recirculates the water from Tank. The water is pumped from Tank through Pipe 1 to Overflow reservoir with mechanism for changing the altitude, which controls the water head using the overflow. The excess water overflows and returns to Tank by means of Pipe 2, while the rest goes through Pipe 3 to Reservoir 1 (2 m heigh, ϕ125 mm inner diameter) and then to Sample reservoir (0.2 m × 0.2 m × 0.5 m) containing squared shape Sample (≈0.2 m × 0.2 m × 0.06 m). After filtrating bottom up through Sample, water overflows to Vessel 1 (0.04 m^3), and then through Drainage pipe 1 (ϕ150 mm) to Vessel 2 (0.04 m^3) placed on Scale of high accuracy (±10 g)—see Figure 4. Prevention of Sample floating and the leakage on Sample sides is described in Supporting Information S1. Vessel 2 is drained by means of Drainage pipe 2 (ϕ150 mm) distributing the water back into Tank.

Laboratory setup in Figure 4 accurately controls the steady-state conditions by means of Overflow reservoir (regardless of the flow pumped from Tank), allowing to impose a wide range of gradients including rather small ones. Drainage pipes 1 and 2 are sufficiently large so the lag time between water overflow from Sample reservoir and its entrance into Vessel 2 is negligible. Note that all Reservoirs are made of plexiglass, while all Pipes are elastic with exception of Drainage pipes 1 and 2 that are plastic.

Before running the test Sample needs to be fully saturated. To do so, Valve 1 and Valve 2 are open, and so as Drainage pipe 2 by removing Cover. Water is left to circulate between 30 min and 1 hr under the high pressure secured by placing Overflow reservoir as high as possible. When the steady state conditions are reached (water level Π_1 is stabilized—see Figure 4) and trapped air is removed, Sample is saturated and the test can start. Overflow reservoir is placed on a position securing desired gradient $\frac{\Delta H_{imp,j}}{\Delta L}$, where $\Delta H_{imp,j}$ is measured manually by the metric scale as the difference between the water level in Piezometer Π_{12} and that in Sample reservoir (Π_2) where water overflows (see Figure 4). By closing Drainage pipe 2 with Cover (see Figure 4), the change of water mass (outflow Q) entering Vessel 2 is measured continuously on Scale until Vessel 2 is almost full. The uniform change of the outflow mass in time indicates constant Q_j value equal to the ratio between the total mass of the outflow and the time required for collecting it. By linking $v_{s,j} = \frac{Q_j}{A_s}$ value with the corresponding gradient $\frac{\Delta H_{imp,j}}{\Delta L}$, jth experimental point is obtained. After removing Cover water almost instantly drains into Tank, and the whole procedure is repeated for a different gradient imposed by changing the altitude of Overflow reservoir. As a result, multiple experimental points (water flux values related to the corresponding gradients) are obtained, and values of K_{sat} and β are determined from the best fit with Forchheimer quadratic law (Equation 1).

19447973, 2023, 7, Downloaded from https://agupubs.onlinelibrary.wiley.com/doi/10.1029/2022WR034158 by INASP/HINARI - SERBIA, Wiley Online Library on [28/11/2023]. See the Terms and Conditions (https://onlinelibrary.wiley.com/terms-and-conditions) on Wiley Online Library for rules of use; OA articles are governed by the applicable Creative Commons License

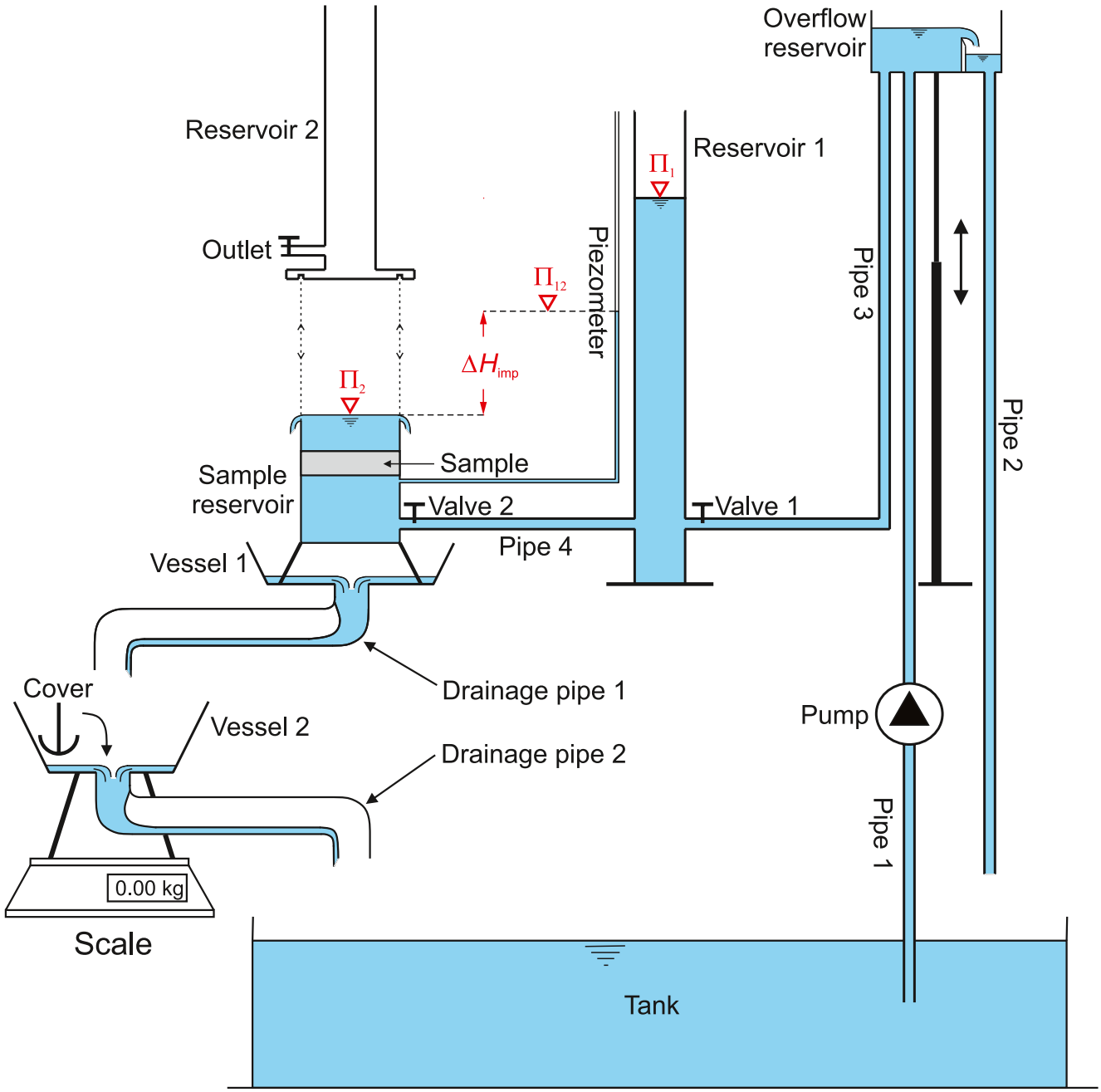

Figure 4. Scheme of the laboratory setup.

3.2. Two-Reservoirs Test

As previously explained, when performing the two-reservoirs test it is desirable to use larger diameter of the pipe connecting two reservoirs (Pipe 4 in Figure 4) to reduce the impact of friction. In this study it was not feasible to use pipes of diameter larger than ϕ19.0 mm due to risk of plexiglass cracking if drilling larger holes on sides of cylindrical shape Reservoir 1. Hence, to reduce the impact of friction, an additional Pipe 4′ (together with Valve 2′) of the same length (L_p = 1.05 m) and the same diameter (ϕ19.0 mm) as Pipe 4 is installed parallel to it to split the flow in two (not presented in Figure 4 due to simplicity).

To perform this test, Reservoir 2 (ϕ125 mm inner diameter) is installed on the top of Sample reservoir (see Figure 4—more details in Supporting Information S1), and hence Π_2 is not constant as in the previous test, but

19447973, 2023, 7, Downloaded from https://agupubs.onlinelibrary.wiley.com/doi/10.1029/2022WR034158 by INASP/HINARI - SERBIA, Wiley Online Library on [28/11/2023]. See the Terms and Conditions (https://onlinelibrary.wiley.com/terms-and-conditions) on Wiley Online Library for rules of use; OA articles are governed by the applicable Creative Commons License

Figure 5. Four investigated pervious paver samples with 0%, 10%, 20% and 30% of solidified wastewater treatment sludge, respectively, going from left to right.

changes within Reservoir 2 as in Figure 1. As for the constant head permeability test, Sample is first saturated. If Reservoir 2 is mobile as in Figure 4, Sample is saturated without it, the same way as in the constant head permeability test. Otherwise, Sample is saturated by filling Reservoirs 1 and 2 with water to the top by opening Valve 1. Once they are filled, Valve 1 is closed and Sample is left laying for some time under the imposed water table. Then, Valve 2 is closed, and Outlet is open to drain the water solely from Reservoir 2. After closing Outlet, the test starts by abruptly opening Valve 2 when water starts flowing from Reservoir 1 into Reservoir 2 due to initially imposed water level difference. Both Π_1 and Π_2 are continuously recorded by means of high-resolution camera (Sony RX10 M2), while Piezometer is not used in this test because Π_{12} data are not necessary for the approach proposed here. The procedure used in Marjanović et al. (2019) and Ljubičić et al. (2020) for extracting the water level data from recordings is applied here, and it is thoroughly described in Supporting Information S2.

3.3. Samples

Four types of lightweight pervious concrete pavers, that have a wide range of applications in a construction field, were investigated in this paper (see Figure 5). Such materials are mostly used for pervious pavements for parking lots and roads, and its main purpose is reduction of the stormwater surface runoff, but also protection from the pollution (Brite/Euram Report, 1994; Hammes et al., 2018; Sambito et al., 2021; Winston et al., 2020). The pavers, whose dimensions are given in Table 1, are made of lightweight aggregate of expanded clay particles (fraction 1–4 mm), cement CEM I 52.5 R used as a binder which is substituted with a solidified wastewater treatment sludge (SWWTS) to a certain extent (see Table 1), and water. According to Govedarica et al. (2022), the porosity of these four samples varies between 0.35 and 0.38. For more details on this material see the aforementioned study.

4. Results

The two-reservoirs test has been performed on four presented paver samples where the proposed semi-analytical solution has been applied to determine the values of K_{sat} and β. To validate the results obtained, the constant head permeability test, which is considered as a reference, has been also performed on each sample. In the following

Table 1
The Percentage of Solidified Wastewater Treatment Sludge Substituting Cement in the Investigated Samples and Their Dimensions

Paver type	Percentage of SWWTS (%)	ΔL (cm)	A_s (cm^2)
Sample 1—Gray paver	0	6.08	19.90 × 19.96
Sample 2—Brown paver	10	5.85	19.85 × 19.95
Sample 3—Red paver	20	5.46	19.95 × 19.98
Sample 4—Green paver	30	5.60	19.92 × 19.92

19447973, 2023, 7, Downloaded from https://agupubs.onlinelibrary.wiley.com/doi/10.1029/2022WR034158 by INASP/HINARI - SERBIA, Wiley Online Library on [28/11/2023]. See the Terms and Conditions (https://onlinelibrary.wiley.com/terms-and-conditions) on Wiley Online Library for rules of use; OA articles are governed by the applicable Creative Commons License

19447973, 2023, 7, Downloaded from https://agupubs.onlinelibrary.wiley.com/doi/10.1029/2022WR034158 by INASP/HINARI - SERBIA, Wiley Online Library on [28/11/2023]. See the Terms and Conditions (https://onlinelibrary.wiley.com/terms-and-conditions) on Wiley Online Library for rules of use; OA articles are governed by the applicable Creative Commons License

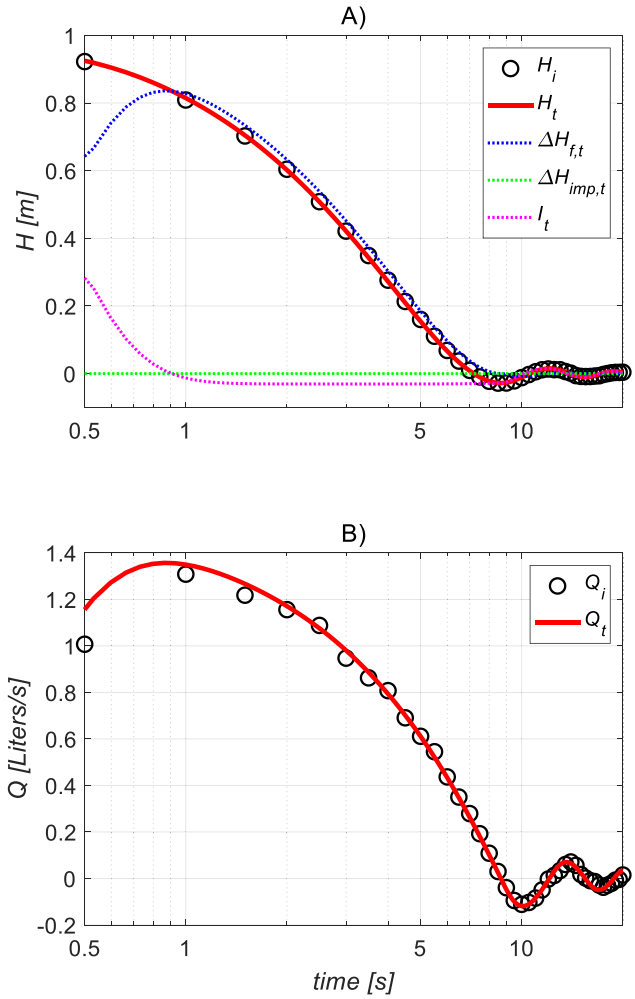

Figure 6. Comparison between (a) the experimental H_i data (empty dots) of the two-reservoirs test without a sample, and the best fitting H_t curve (Equation 24) obtained for $\xi_{tot} = 1.70$ ($K_{sat} = 1 \times 10^9$ m/s and $\beta = 1 \times 10^{-9}$ s^2/m^2 are not calibrated); (b) the experimental Q_i data (Equation 30—empty dots) and the simulated Q_t (Equation 20) for the same parameter values.

text are presented results of both tests and their comparison, as well as the comparison with the falling head permeability approach.

4.1. Data of the Two-Reservoirs Test

To determine values of K_{sat} and β from the two-reservoirs test, it is necessary first to define r_Q controlling $\Delta H_{f,j}$ (see Appendix A). To do so, the test is performed with empty laboratory setup (no sample into Sample reservoir) the same way as explained in Section 3.2, and Equation 24 is fitted with experimental H_i data by adjusting solely friction coefficient ξ_{tot} contributing to r_Q (see Equation A1.4 in Appendix A). In Figure 6a with empty dots are presented measured H_i values, where $H_0 = 0.978$ m and $Q_0 = 0$ L/s, captured by camera every 0.5 s, while with red solid line is presented the best fitting Equation 24 obtained for $\xi_{tot} = 1.70$. In this case $K_{sat} = 1 \times 10^9$ m/s and $\beta = 1 \times 10^{-9}$ s^2/m^2 are not calibrated since they simulate infinitely permeable sample (or no sample). According to the literature, standard value of ξ_{tot} for a pipe connecting two reservoirs side by side (Pipes 4 and 4′ in this case) is about 1.50, while value $\xi_{tot} = 1.70$ is due to Valve 2 which locally reduces the pipe diameter (even when open), and hence creates an additional energy loss. Besides H_t, in Figure 6a are also presented $\Delta H_{f,t}$ (blue dotted line), $\Delta H_{imp,t}$ (green dotted line) and I_t (magenta dotted line), where $\Delta H_{imp,t}$ is zero because sample is infinitely permeable. Since only $\Delta H_{f,t}$ opposes H_t, non-negligible oscillations of H_t can be observed in Figure 6a, where the absolute minimal I_t value is approximately 3.5 cm. In Figure 6b is presented comparison between Q_t (red solid line—Equation 20) and Q_i data (empty dots) obtained from H_i measurements as:

$$Q_i = \frac{H_{i+1} - H_{i-1}}{t_{i+1} - t_{i-1}} A_e \tag{30}$$

The agreement between H_t and H_i, but also Q_t and Q_i, for $\xi_{tot} = 1.70$ is excellent ($R^2 = 0.9999$, RMSE $= 2.6 \times 10^{-3}$ m). It should be emphasized that if using Pipes 4 and 4′ to divide Q_t by half and to transfer the water with less energy losses, it is necessary to account for some modifications in the calculation process. Hence, following Equation 8 $\Delta H_{f,t} = r_Q \frac{Q_t}{2}\left|\frac{Q_t}{2}\right| = \frac{r_Q}{4} Q_t |Q_t|$, where r_Q is calculated for $\left|\frac{Q_t}{2}\right|$ instead of $|Q_t|$ by means of Equation A1.4 ($\Delta H_{11,t}$ and $\Delta H_{22,t}$ are ignored due to large A_{c1} and A_{c2}). Also, since $A_{c1} = A_{c2}$ and $\Delta L = 0$ (there is no sample), c_t is constant and equal to $\frac{\Pi_{1,0} + \Pi_{2,0} - \Delta L}{g A_{c1}} + \frac{L_p}{2 g A_p} = 187.76$ s^2/m^2.

After estimating value of ξ_{tot}, r_Q is fully defined for every Q_t value. Hence, solely values of K_{sat} and β for Samples 1 to 4 are to be determined from H_i measurements obtained when running the test with Sample inside Sample reservoir. In Figure 7 are presented comparisons between the calibrated H_t curves and the experimental H_i data for all Samples, together with calculated $\Delta H_{f,t}$ (dotted blue line), $\Delta H_{imp,t}$ (dotted green line) and I_t (dotted magenta line) components, while in Figure 8 are presented comparisons between the corresponding Q_t and Q_i data. The determined values of K_{sat} and β provide excellent agreement between H_t and H_i ($R^2 > 0.9995$ and RMSE $< 6.5 \times 10^{-3}$ m—see Table 2), but also Q_t and Q_i data, for all Samples. Since only two physically based parameters are to be calibrated (K_{sat} and β), their values are manually adjusted to secure the highest possible R^2 score (Equation 28), but also sufficiently low RMSE values (Equation 29). The calibration can be also performed by means of a certain optimization tool, but since K_{sat} and β have clear physical background and affect differently the behavior of Equation 24, where K_{sat} is dominant at low Q_t, and β at the high-velocity flow, it is more convenient to adjust their values manually.

Note that in all simulations, including the one with infinitely permeable sample, the aforementioned criterium $\Delta t = T/100$ is used for the time interval selection, where $T = 2\pi\sqrt{\frac{L_p A_e}{2 g A_p}} \approx 6.5$ s, and hence $\Delta t = 0.065$ s. Also,

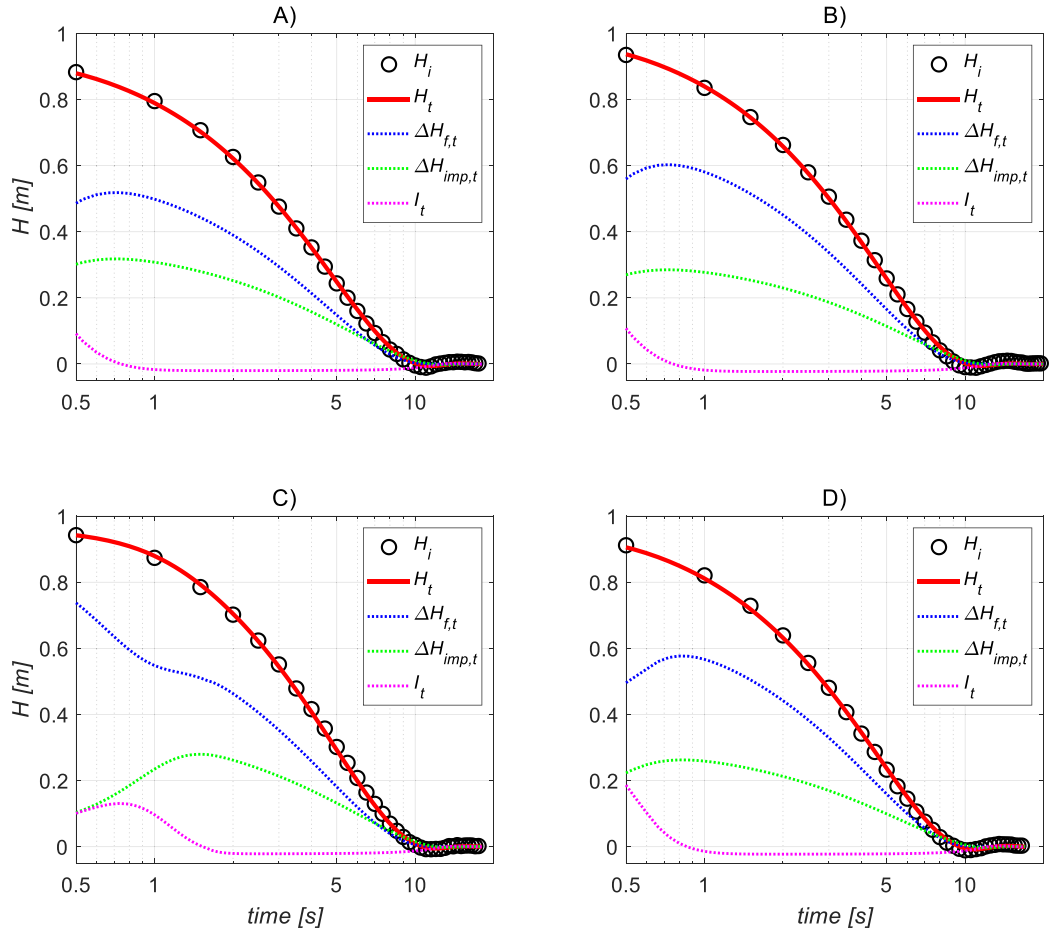

Figure 7. Comparison between the experimental H_i data (empty dots) of the two-reservoirs test with a sample, and the simulated H_t data (Equation 24—red solid line) for (a) Sample 1 (0% SWWTS), (b) Sample 2 (10% SWWTS), (c) Sample 3 (20% SWWTS), (d) Sample 4 (30% SWWTS). In each graph are also presented $\Delta H_{f,t}$ (blue dotted line), $\Delta H_{\mathrm{imp},t}$ (green dotted line) and I_t (magenta dotted line).

for all Samples $Q_0 = 0$ L/s, while $c_t = \frac{\Pi_{1,0}+\Pi_{2,0}-\Delta L}{gA_{c1}} + \frac{L_p}{2gA_p} = 186.75 \pm 0.25$ s^2/m^2 depending on the specific values of $\Pi_{1,0}$, $\Pi_{2,0}$, and ΔL, where $\frac{L_p}{2gA_p}$ contributes to c_t value with more than 95% ($\frac{n\Delta L}{gA_s} \approx 0.05$ s^2/m^2 is negligible for all Samples).

Compared to Figure 6 where $\Delta H_{f,t}$ is the only resistance force, in Figure 7 values of $\Delta H_{f,t}$ are significantly mitigated because Sample reduces the flow rate and creates an additional resistance force $\Delta H_{\mathrm{imp},t}$. Due to stronger resistance, I_t is also reduced compared to Figure 6, which is manifested with more damped oscillations of H_t. The absolute minimal value of I_t for all Samples is between 2.2 and 2.4 cm, which is about 30% lower compared to the test without a sample (Figure 6), but still considerable. Note that $\Delta H_{f,t}$ is still dominant over $\Delta H_{\mathrm{imp},t}$ even though two pipes of diameter ϕ19 mm are used to connect Reservoirs 1 and 2.

4.2. Comparison With the Constant Head Permeability Data

In Figure 9 with empty dots are presented results of the constant head permeability test obtained by applying the procedure from Section 3.1 for nine different gradients $\frac{\Delta H_{\mathrm{imp},j}}{\Delta L}$ ($j = 1, 2, \ldots 9$). Depending on the gradient value, it takes 30–120 s to collect between 30 and 40 L and fill Vessel 2, which means about 300 L of water per sample. Clearly, this would not be feasible without circulation of water from Tank. Values of K_{sat} and β are obtained by fitting Equation 1 with the experimental data (dashed line in Figure 9), and they are presented in Table 2.

19447973, 2023, 7, Downloaded from https://agupubs.onlinelibrary.wiley.com/doi/10.1029/2022WR034158 by INASP/HINARI - SERBIA, Wiley Online Library on [28/11/2023]. See the Terms and Conditions (https://onlinelibrary.wiley.com/terms-and-conditions) on Wiley Online Library for rules of use; OA articles are governed by the applicable Creative Commons License

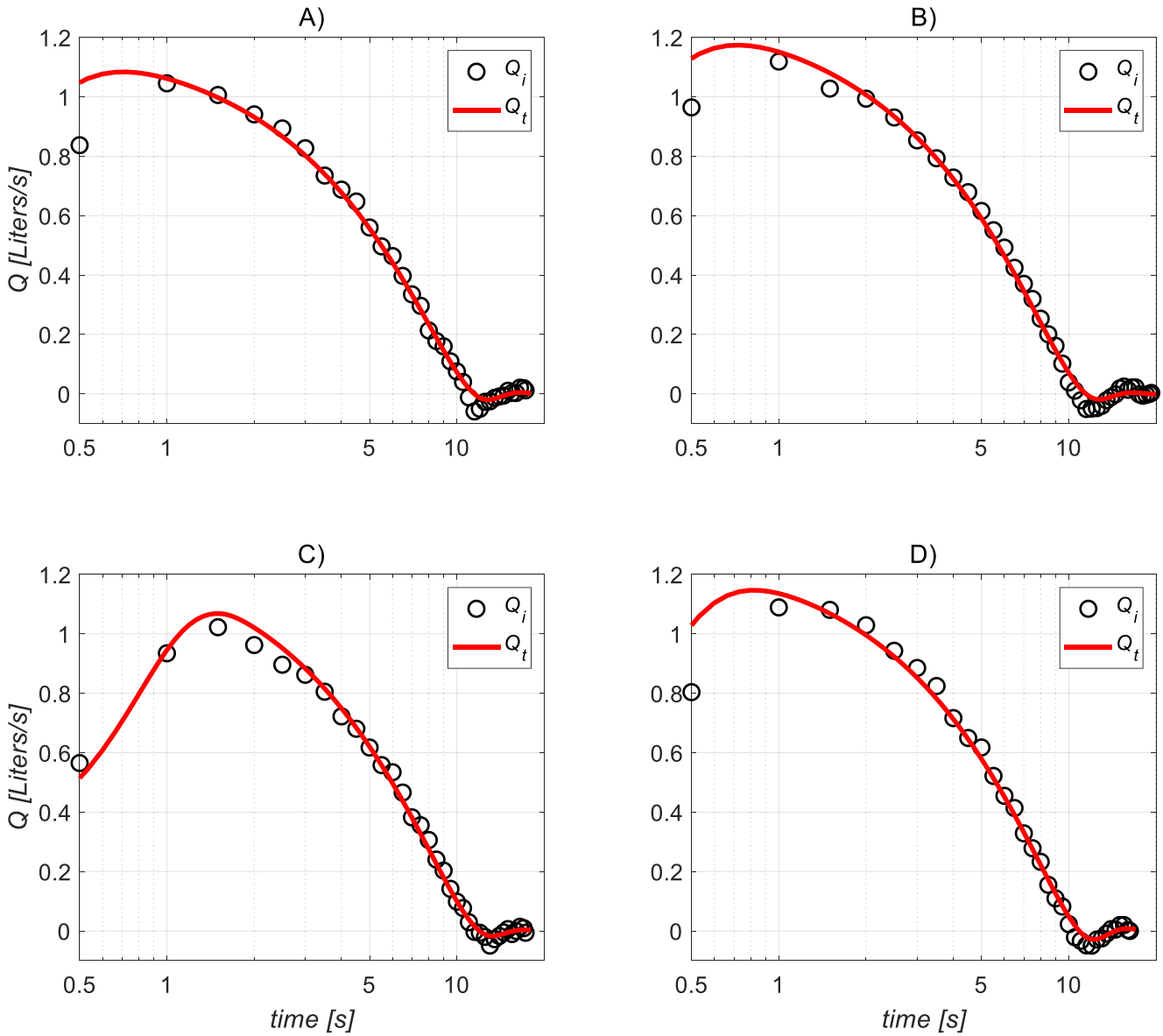

Figure 8. Comparison between the experimental Q_i data (Equation 30—empty dots) of the two-reservoirs test with a sample, and the simulated Q_t data (Equation 20—red solid line) for (a) Sample 1 (0% SWWTS), (b) Sample 2 (10% SWWTS), (c) Sample 3 (20% SWWTS), (d) Sample 4 (30% SWWTS).

Table 2
Results of the Two-Reservoirs Test and the Constant Head Permeability Test

		Sample 1	Sample 2	Sample 3	Sample 4
Two-reservoirs test	K_{sat} (m/s)	1.29×10^{-2}	1.15×10^{-2}	1.06×10^{-2}	1.39×10^{-2}
	β (s^2/m^2)	3.120×10^{3}	1.850×10^{3}	2.550×10^{3}	2.300×10^{3}
	R^2 (–)	0.9997	0.9995	0.9998	0.9996
	RMSE (m)	4.8×10^{-3}	6.3×10^{-3}	4.8×10^{-3}	6.0×10^{-3}
Constant head permeability test	K_{sat} (m/s)	1.18×10^{-2}	1.16×10^{-2}	1.13×10^{-2}	1.34×10^{-2}
	β (s^2/m^2)	3.658×10^{3}	1.847×10^{3}	2.129×10^{3}	2.528×10^{3}

19447973, 2023, 7, Downloaded from https://agupubs.onlinelibrary.wiley.com/doi/10.1029/2022WR034158 by INASP/HINARI - SERBIA, Wiley Online Library on [28/11/2023]. See the Terms and Conditions (https://onlinelibrary.wiley.com/terms-and-conditions) on Wiley Online Library for rules of use; OA articles are governed by the applicable Creative Commons License

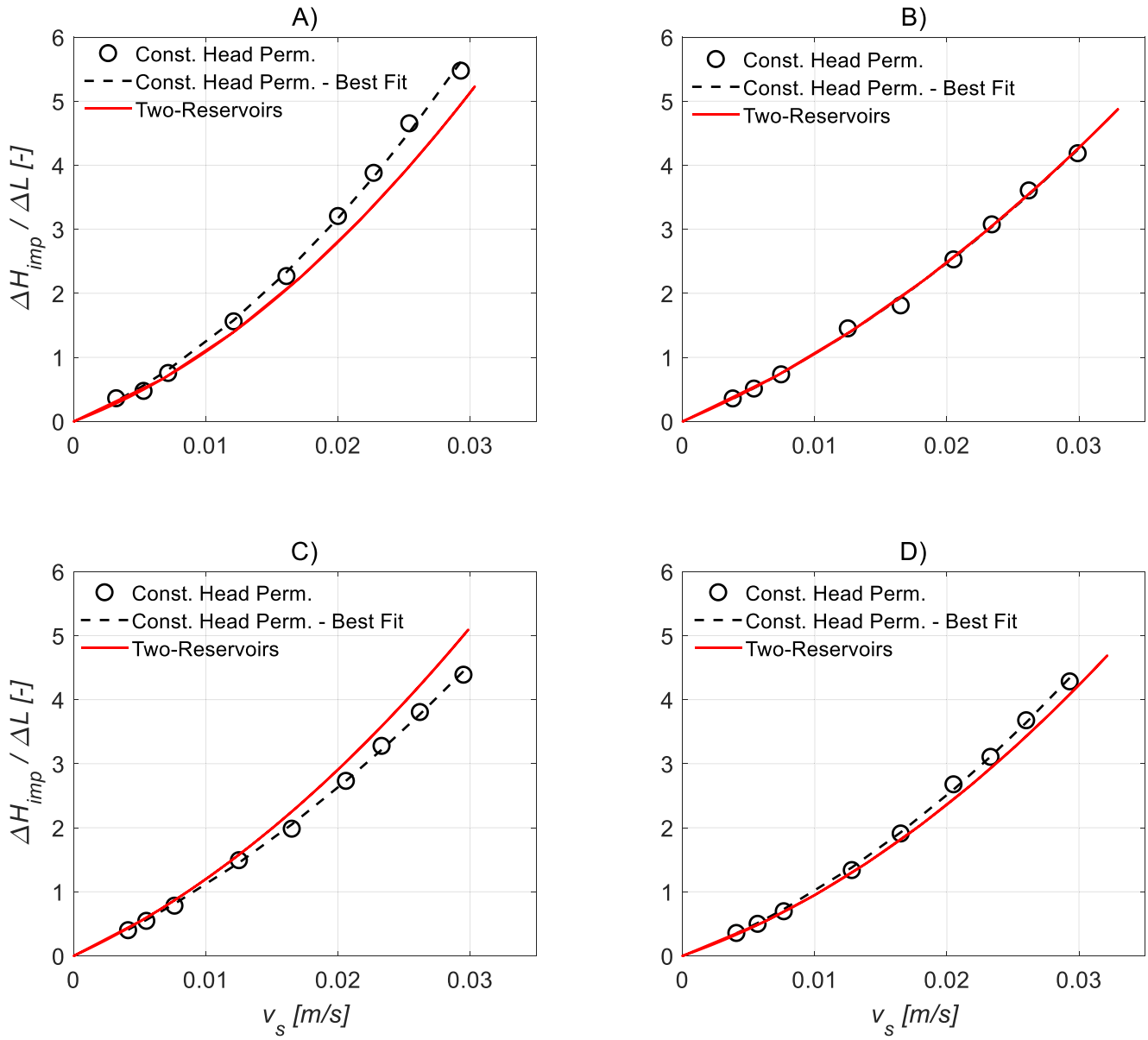

Figure 9. Comparison between the constant head permeability data (empty dots—experimental points; dashed line—best fitting Equation 1) and the results of the two-connected reservoirs test (solid line) for (a) Sample 1 (0% SWWTS), (b) Sample 2 (10% SWWTS), (c) Sample 3 (20% SWWTS), (d) Sample 4 (30% SWWTS).

To compare the results of two different tests performed here, it is convenient to reduce them to a common form. To do so, the calculated $\Delta H_{\mathrm{imp},t}$ values from Figure 7 (green dotted line) are linked with the corresponding values of Q_t ($v_s = \frac{Q_t}{A_s}$) from Figure 8 (solid line), where both components relate to same t, and the data obtained are presented in Figure 9 with solid line. Figure 9 shows the results of the two-reservoirs test describe the constant head permeability measurements quite well at small v_s when K_{sat} is still dominant due to Darcy linear behavior, while certain deviation occurs at higher v_s when the quadratic component of Forchheimer law becomes considerable. As explained before, this is mainly because the semi-analytical solution is less sensitive to β when $\Delta H_{f,t}$ is dominant over $\Delta H_{\mathrm{imp},t}$, so it is difficult to make clear distinction between the impacts of r_Q and b. Still, the overall agreement between the results of two test is satisfactory, and both tests provide the highest β values in case of Sample 1 (see Table 2) which shows slightly lower permeability, especially at higher gradients, than that of Samples 2, 3, and 4 containing certain percentage of SWWTS replacing cement.

19447973, 2023, 7, Downloaded from https://agupubs.onlinelibrary.wiley.com/doi/10.1029/2022WR034158 by INASP/HINARI - SERBIA, Wiley Online Library on [28/11/2023]. See the Terms and Conditions (https://onlinelibrary.wiley.com/terms-and-conditions) on Wiley Online Library for rules of use; OA articles are governed by the applicable Creative Commons License

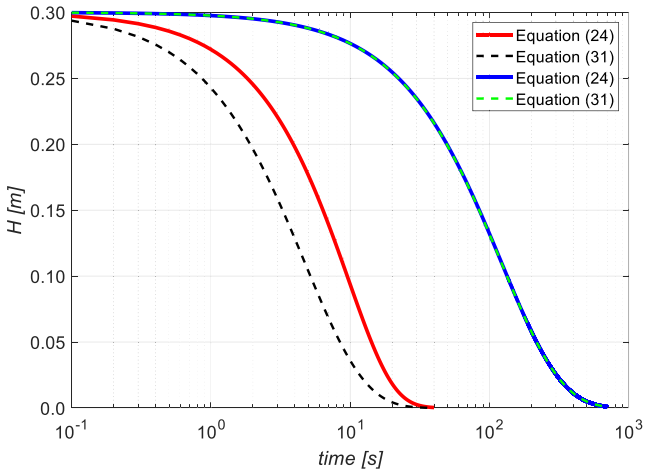

Figure 10. Comparison between Equations 24 and 31 for: $K_{sat} = 1.29 \times 10^{-2}$ m/s and $\beta = 3{,}120$ s^2/m^2 (red solid line and black dashed line); $K_{sat} = 5 \times 10^{-4}$ m/s and $\beta = 3{,}120$ s^2/m^2 (blue solid line and green dashed line).

4.3. Comparison With the Falling Head Permeability Test

To compare the proposed two-reservoirs approach with the conventional falling head permeability approach (FprEN 12697-19:2019 E, 2019), the input data for Equation 24 need to be adapted. To cope with the standard falling head laboratory setup from FprEN 12697-19:2019 E (2019), where 0.3 m of water column height filtrates through the sample top to bottom and overflows from the water bath surrounding the column into the collecting reservoir, $A_{c,2}$ is set to infinity (e.g., 1×10^9 m^2) to simulate the constant downstream water head $\Pi_{2,t} = \Pi_{2,0} = 0$, L_p and ξ_{tot} are set to zero because water is not transferred through the pipe and there are no local energy losses, while $A_{c1} = A_s$. Hence, $r_Q = 0$ according to Equation A1.4 in Appendix A, while c_t reduces to $c_t = \frac{\Pi_{1,t}}{gA_{c1}} + \frac{n\Delta L}{gA_s} = \frac{H_t + n\Delta L}{gA_s}$ because $H_t = \Pi_{1,t} - \Pi_{2,t} = \Pi_{1,t}$ (value of $n = 0.35$ is used). By adopting the mentioned modifications, the calculation is performed following calculation steps 1 to 6 as before, and the results obtained are compared with the standard equation describing the falling head permeability data:

$$H_t = H_0 e^{-\frac{K_{sat} A_s t}{\Delta L A_{c,1}}} \tag{31}$$

Equation 31 is identical as in Das (2002) and Bear (1972) but presented as a continuous function of time. Figure 10 illustrates the comparison between Equations 24 and 31 performed for two different scenarios. In the first case, values of $K_{sat} = 1.29 \times 10^{-2}$ m/s and $\beta = 3{,}120$ s^2/m^2 for Sample 1 are used (see Table 2), while in the second case K_{sat} is reduced to 5×10^{-4} m/s to simulate less permeable material. The reason for not changing β while reducing K_{sat} is because its value is irrelevant at low flow rate Q_t when K_{sat} is dominant (almost identical results are obtained for β close to zero). For highly pervious materials such as Sample 1, Equation 31 underestimates the material's water permeability (red solid line in Figure 10), as stated by Sandoval et al. (2017), because it shows more rapid drop of H_t than Equation 24 (black dashed line) for the same value of $K_{sat} = 1.29 \times 10^{-2}$ m/s. This is because Equation 31 ignores the inertial force I_t, even though a considerable change of outflow in time occurs, as well as the high-velocity flow through the sample described through Forchheimer's coefficient β. As K_{sat} reduces and the test duration extends, the change of outflow in time and the outflow itself mitigate, and hence the impacts of I_t and β reduce. This is in better agreement with the assumptions of the falling head permeability test, which is manifested with almost identical results obtained from Equations 24 and 31 (blue solid line and green dashed line, respectively).

5. Conclusion

This paper presents an innovative approach for determination of the water permeability of a saturated porous medium. It implies (a) an experimental procedure with porous sample placed between two connected reservoirs, where water flow is triggered by means of the imposed water level difference, and (b) a new semi-analytical solution describing the damped water level oscillations in these reservoirs by considering the fluid mass inertia and the high-velocity flow through the porous sample (Forchheimer's quadratic law) and the laboratory setup. This semi-analytical expression assumes constant water pressure and gravity component (driving force) over a sufficiently short time interval Δt estimated from the theoretical oscillation period for undamped oscillations, and hence the iterative calculation is performed consecutively at each Δt. The parameters describing the water permeability of a porous medium, saturated hydraulic conductivity K_{sat} and Forchheimer's coefficient β, are determined from the best fit between the proposed semi-analytical solution and the measured water level change in two connected reservoirs. To facilitate determination of K_{sat} and β by making the solution more sensitive to them, it is necessary to reduce the impact of the friction force as much as possible (e.g., increasing diameter of the pipe connecting two reservoirs), giving more influence to the impedance of the sample. To do so, it is highly recommended to estimate the adequate installation pipe dimensions based on the simulation results performed with the assumed permeability parameters of the investigated porous medium.

19447973, 2023, 7, Downloaded from https://agupubs.onlinelibrary.wiley.com/doi/10.1029/2022WR034158 by INASP/HINARI - SERBIA, Wiley Online Library on [28/11/2023]. See the Terms and Conditions (https://onlinelibrary.wiley.com/terms-and-conditions) on Wiley Online Library for rules of use; OA articles are governed by the applicable Creative Commons License

19447973, 2023, 7, Downloaded from https://agupubs.onlinelibrary.wiley.com/doi/10.1029/2022WR034158 by INASP/HINARI - SERBIA, Wiley Online Library on [28/11/2023]. See the Terms and Conditions (https://onlinelibrary.wiley.com/terms-and-conditions) on Wiley Online Library for rules of use; OA articles are governed by the applicable Creative Commons License

The presented approach was tested on four pervious paver samples (0.06 m heigh and 0.04 m^2 quadratic base area, approximately) containing different percentages of SWWTS (0%, 10%, 20%, and 30%) as a replacement for cement. To determine K_{sat} and β for all samples, a modular laboratory setup has been designed to cope with the two-reservoirs test and with the constant head permeability test which is considered as a reference. In case of the two-reservoirs test the proposed semi-analytical solution has been fitted with the water level measurements captured by means of high-resolution camera, where excellent agreement between simulated and measured data is obtained for all samples. The determined values of K_{sat} are between 1.05 and 1.4×10^{-2} m/s, while β takes values between 1,850 and 3,150 s^2/m^2. These results are in agreement with those of the constant head permeability test, which confirms the reliability of the newly proposed approach, but also emphasizes its advantage in terms of efficiency and water savings. Furthermore, the presented approach has been compared with the conventional falling head permeability approach, and the results showed the novel semi-analytical solution reduces to the standard falling head formula for materials of lower permeability, while in case of highly permeable materials the falling head approach underestimates K_{sat} due to ignorance of the inertial force and the quadratic component of Forchheimer's law. Besides the efficiency and the accuracy of the presented approach, one of its main advantages is simple application which implies only the water level measurements in two reservoirs.

Appendix A

According to Darcy-Weisbach equation (Nakayama & Boucher, 1998), the energy or water head loss $\Delta H_{f,t}$ due to friction along the pipe of length L_p [L] and diameter D_p [L] is a function of a water flux v_p [L/T] in the pipe:

$$\Delta H_{f,t} = \left(\lambda \frac{L_p}{D_p} + \xi_{\text{tot}}\right) \frac{{v_p}^2}{2g} \tag{A1.1}$$

where λ is Darcy-Weisbach friction factor [−] which depends on Reynolds number $R_e = \frac{v_p D_p}{\nu}$, with ν being the kinematic viscosity of fluid [L^2/T] ($\nu = 1 \times 10^{-6}$ m^2/s for water at 20°C), while ξ_{tot} is the friction coefficient [−] accounting for the local energy losses due to different obstacles along the flow or changes in pipe geometry. The relationship between λ and R_e is well documented in the literature with the family of different experimentally determined curves (Nikuradse, 1933), each related to a specific value of the relative roughness of a pipe. These experimental data are well described with various empirical expressions (Das et al., 2015; Eismann & Adams, 2018, etc.) valid over different ranges of R_e values, which allows efficient and accurate determination of λ for different water velocities v_p and pipe geometry. One of the commonly used expressions which covers wide range of R_e numbers (from 2,000 to 10^5) without using relative roughness of the pipe is proposed by Blasius (1913):

$$\lambda = 0.3164\, {R_e}^{-0.25} \tag{A1.2}$$

By introducing $R_e = \frac{v_p D_p}{\nu}$ into Equation A1.2, and then back into Equation A1.1 together with $v_p = \frac{Q_t}{A_p} = \frac{4Q_t}{{D_p}^2 \pi}$, the following is obtained:

$$\Delta H_{f,t} = r_Q {Q_t}^2 \tag{A1.3}$$

where r_Q is the friction factor from the main text, determined as below after substituting $g = 9.81$ m/s^2 and $\pi = 3.1416$:

$$r_Q = 0.0246 \frac{L_p \nu^{0.25}}{{D_p}^{4.75}} {Q_t}^{-0.25} + 0.0826 \frac{\xi_{\text{tot}}}{{D_p}^4} \tag{A1.4}$$

Note that $\Delta H_{f,t} = \Delta H_{1,t}$ is assumed here, while the energy losses $\Delta H_{11,t}$ and $\Delta H_{22,t}$ are neglected (see Section 2.1 in the main text). This is justified when the cross-sectional areas of Reservoirs 1 and 2 are significantly larger than that of the pipe connecting them (usually the case). Otherwise, r_Q is calculated for each section separately using Equation A1.4, and the values are summed.

Appendix B

Since Equation 12 from the main text has no analytical solution, it is solved numerically by writing it in the discrete form as:

$$-c_t A_e \frac{H_t - 2H_{t-\Delta t} + H_{t-2\Delta t}}{\Delta t^2} - aA_e \frac{H_t - H_{t-\Delta t}}{\Delta t} - (r_Q + b){A_e}^2 \frac{H_t - H_{t-\Delta t}}{\Delta t} \left|\frac{dH}{dt}\right|^* - H_t = 0 \quad \text{(B1.1)}$$

where $\frac{d^2H}{dt^2} \approx \frac{\left(\frac{dH}{dt}\right)_t - \left(\frac{dH}{dt}\right)_{t-\Delta t}}{\Delta t} \approx \frac{\frac{H_t - H_{t-\Delta t}}{\Delta t} - \frac{H_{t-\Delta t} - H_{t-2\Delta t}}{\Delta t}}{\Delta t} = \frac{H_t - 2H_{t-\Delta t} + H_{t-2\Delta t}}{\Delta t^2}$ and $\left|\frac{dH}{dt}\right|^*$ is the derivative value taken from the previous iteration. After putting together different terms related to H_t, $H_{t-\Delta t}$, and $H_{t-2\Delta t}$, respectively, the following is obtained:

$$H_t\left(\frac{aA_e}{\Delta t} + \frac{(r_Q + b){A_e}^2}{\Delta t}\left|\frac{dH}{dt}\right|^* + \frac{c_t A_e}{\Delta t^2} + 1\right) - H_{t-\Delta t}\left(\frac{(r_Q + b){A_e}^2}{\Delta t}\left|\frac{dH}{dt}\right|^* + \frac{aA_e}{\Delta t} + \frac{2c_t A_e}{\Delta t^2}\right) + H_{t-2\Delta t}\frac{c_t A_e}{\Delta t^2} = 0 \quad \text{(B1.2)}$$

Finally, H_t is expressed as:

$$H_t = \frac{H_{t-\Delta t}\left(\frac{(r_Q + b){A_e}^2}{\Delta t}\left|\frac{dH}{dt}\right|^* + \frac{aA_e}{\Delta t} + \frac{2c_t A_e}{\Delta t^2}\right) - H_{t-2\Delta t}\frac{c_t A_e}{\Delta t^2}}{\frac{aA_e}{\Delta t} + \frac{(r_Q + b){A_e}^2}{\Delta t}\left|\frac{dH}{dt}\right|^* + \frac{c_t A_e}{\Delta t^2} + 1} \quad \text{(B1.3)}$$

To calculate H_t it is necessary to apply iterative procedure where after applying Equation B1.3 the term $\left|\frac{dH}{dt}\right|^* = \left|\frac{H_t - H_{t-\Delta t}}{\Delta t}\right|$ is recalculated and introduced back into Equation B1.3 to determine new value of H_t. This is repeated iteratively until the absolute difference between H_t values in two consecutive iterations becomes negligible. Initially, $\left|\frac{dH}{dt}\right|^* = \left|\frac{H_{t-\Delta t} - H_{t-2\Delta t}}{\Delta t}\right|$ is adopted from the previous time step (index $t - \Delta t$), while for $t = \Delta t$ the value $H_{t-2\Delta t} = H_{t-\Delta t} = H_0$. Also, the flow rate is calculated as $Q_t = A_e \frac{H_t - H_{t-\Delta t}}{\Delta t}$ and is used to determine r_Q value at each iteration.

Appendix C

The proposed semi-analytical solution is interval-based and as such it depends on the calculation step interval Δt. Figure C1 illustrates results obtained for different Δt values and for variety of K_f and β values corresponding to highly pervious materials, where oscillations of H_t occur. In Figure C1 graphs of the same column have identical β but different K_f, whereas graphs of the same row have identical K_f but different β. The sample flow resistance mitigates the amplitudes of H_t, but also extends the oscillation period T^* compared to the undamped oscillations period $T = 3.66$ s (see caption of Figure C1). Since T^* is always higher than T, defining Δt as a percentile of T may be considered a conservative criterion, certainly on the safety side.

Stability wise, it is important to ensure the calculation error does not increase in time. Since the proposed solution is semi-analytical and highly non-linear, the conventional stability analysis (Hirsch, 2007) applied for numerical schemes is not suitable here. Still, the calculation error at each time step can be computed from Equation 7 as $\text{err} = H_t - \left(\Delta H_{f,t} + \Delta H_{\text{imp},t}\right) - I_t$, where each component on the right hand side is calculated from Equations 8, 9, 24 and 27, respectively. Due to analytical nature of the proposed solution, the value of *err* at each Δt corresponds to the difference between H_t values in two consecutive iterations. If the solution converges, the absolute value of *err* at each time step must be lower than the tolerance defined as the criteria for convergence (1×10^{-6} m in this case). For all Δt values and all combinations of K_f and β from Figure C1 the value of *err* decreases as H_t approaches zero, and hence the proposed solution is considered as stable for these Δt. Note that in some cases Δt is temporarily reduced as explained in the main text to secure the solution convergence.

However, not all Δt values provide equally accurate results. If using $\Delta t = T/4$ or $\Delta t = T/20$, most of the time the calculation error (*err*) is rather close to the tolerance (1×10^{-6} m in this case), whereas for $\Delta t = T/100$ or $\Delta t = T/500$ values of *err* are more than two orders of magnitude lower. Similarly, results presented in Figure C1 show that H_t curves related to $\Delta t = T/100$ or $\Delta t = T/500$ (dashed and solid lines, respectively) are almost identical,

19447973, 2023, 7, Downloaded from https://agupubs.onlinelibrary.wiley.com/doi/10.1029/2022WR034158 by INASP/HINARI - SERBIA, Wiley Online Library on [28/11/2023]. See the Terms and Conditions (https://onlinelibrary.wiley.com/terms-and-conditions) on Wiley Online Library for rules of use; OA articles are governed by the applicable Creative Commons License

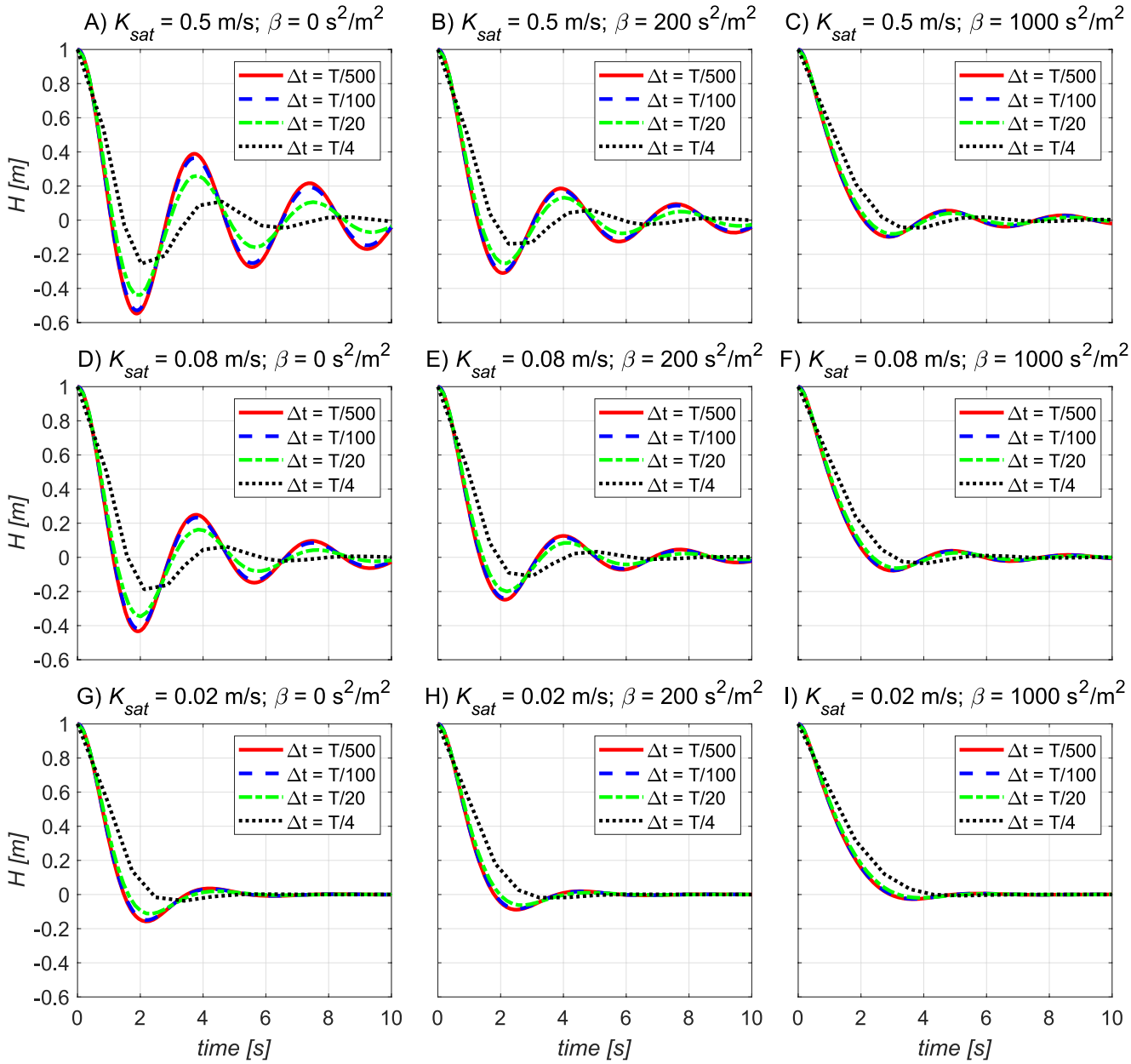

Figure C1. Results of the proposed semi-analytical solution (H_t) for different Δt values ($\Delta t = T/500$, $\Delta t = T/100$, $\Delta t = T/20$, $\Delta t = T/4$) and different combinations of K_{sat} (2×10^{-2}–5×10^{-1} m/s) and β (0–1,000 s^2/m^2). The model outcomes are provided for the following input data: H_0 = 1 m, Q_0 = 0 L/s, ΔL = 0.06 m, A_s = 0.04 m^2, **$A_p = 2 \times 10^{-3}$ m^2(ϕ50.8 mm),** L_p = 1.1 m, $A_{c,1} = A_{c,2}$ = 0.0123 m^2 (ϕ125 mm), and $T = 2\pi\sqrt{\frac{L_p A_c}{g A_p}} = 3.66$ s.

while H_t values for $\Delta t = T/4$ and $\Delta t = T/20$ (dotted and dash-dotted lines, respectively) are mitigated and postponed. Also, the number of iterations required for the solution to converge increases with the Δt increase. Hence, more than 50 iterations per time step are required when using $\Delta t = T/4$, whereas three iterations (the recommended number of iterations) are sufficient for $\Delta t = T/100$ and $\Delta t = T/500$. Based on everything mentioned it can be concluded that, regardless of the material's permeability, the criterion $\Delta t = T/100$ is good enough to provide both accurate and stable calculation of H_t using the proposed semi-analytical solution.

19447973, 2023, 7, Downloaded from https://agupubs.onlinelibrary.wiley.com/doi/10.1029/2022WR034158 by INASP/HINARI - SERBIA, Wiley Online Library on [28/11/2023]. See the Terms and Conditions (https://onlinelibrary.wiley.com/terms-and-conditions) on Wiley Online Library for rules of use; OA articles are governed by the applicable Creative Commons License

Data Availability Statement

All the relevant information necessary for reproducing the results from this paper can be found in the text, while the experimental data are deposed in Zenodo repository (Stanić et al., 2023a), as well as the Matlab codes that were used for creating Figures and performing different kinds of analysis (Stanić et al., 2023b).

Acknowledgments
This research was funded by the Science Fund of the Republic of Serbia through the IDEJE national project Ø-Waste-Water (No 7737365) and by the European Union-funded project euPOLIS under the Horizon 2020 program H2020-EU.3.5.2 (No 869448). Authors greatly acknowledge the factory "Promobet—betonski proizvodi" for providing the testing samples of pervious paver investigated in this study. Also, special acknowledgment to the technician from Department for Hydraulics and Environmental Engineering Ivor Kokotović who had a significant contribution in designing and developing the experimental setup used for this research.

References

Bagarello, V., Iovino, M., & Elrick, D. (2004). A simplified falling-head technique for rapid determination of field-saturated hydraulic conductivity. *Soil Science Society of America Journal*, *68*(1), 66–73. https://doi.org/10.2136/sssaj2004.6600

Beach, D. N. H., McCray, J. E., Lowe, K. S., & Siegrist, R. L. (2005). Temporal changes in hydraulic conductivity of sand porous media biofilters during wastewater infiltration due to biomat formation. *Journal of Hydrology*, *311*(1–4), 230–243. https://doi.org/10.1016/j.jhydrol.2005.01.024

Bear, J. (1972). *Dynamics of fluids in porous media* (p. 764). American Elsevier. (also published by Dover Publications, 1988).

Beryani, A., Goldstein, A., Al-Rubaei, A. M., Viklander, M., Hunt, W. F., III, & Blecken, G. T. (2021). Survey of the operational status of twenty-six urban stormwater biofilter facilities in Sweden. *Journal of Environmental Management*, *297*, 113375. https://doi.org/10.1016/j.jenvman.2021.113375

Blasius, H. (1913). Das Aehnlichkeitsgesetz bei Reibungsvorgängen in Flüssigkeiten. In *Mitteilungen über Forschungsarbeiten auf dem Gebiete des Ingenieurwesens* (Vol. 1–41). Springer. https://doi.org/10.1007/978-3-662-02239-9_1

Bouma, J. (1982). Measuring the hydraulic conductivity of soil horizons with continuous macropores. *Soil Science Society of America Journal*, *46*(2), 438–441. https://doi.org/10.2136/sssaj1982.03615995004600020047x

Bouzouidja, R., Cannavo, P., Bodénan, P., Gulyás, Á., Kiss, M., Kovács, A., et al. (2021). How to evaluate nature-based solutions performance for microclimate, water and soil management issues—Available tools and methods form Nature4Cities European project results. *Ecological Indicators*, *125*, 107556. https://doi.org/10.1016/j.ecolind.2021.107556

Brite/Euram Report. (1994). *Surface properties of concrete roads in accordance with traffic safety and reduction of noise* (p. 138). Brite/Euram (Project BE3415.

Burdine, N. T. (1953). Relative permeability calculations from pore size distribution data. *Journal of Petroleum Technology*, *5*(03), 71–78. https://doi.org/10.2118/225-g

Clemente, R. S., De Jong, R., Hayhoe, H. N., Reynolds, W. D., & Hares, M. (1994). Testing and comparison of three unsaturated soil water flow models. *Agricultural Water Management*, *25*(2), 135–152. https://doi.org/10.1016/0378-3774(94)90041-8

Das, B. M. (2002). *Soil mechanics laboratory manual* (6th ed.). Oxford University Press.

Das, B. M., Sarma, B., & Das, M. M. (2015). Error analysis of friction factor formulae with respect to Colebrook-White equation. *International Journal of Science and Research*, *6*(3), 2105–2109.

Diminescu, M. A., Dumitran, G. E., & Vuță, L. I. (2019). Experimental methods to determine the hydraulic conductivity. In *E3S web of conference* (Vol. 85, p. 06010). https://doi.org/10.1051/e3sconf/20198506010

Dirksen, C. (1999). *Soil physics measurements*. Catena, Verlag.

dos Santos, R. C. V., Vargas, M. M., Timm, L. C., Beskow, S., Siqueira, T. M., Mello, C. R., et al. (2021). Examining the implications of spatial variability of saturated soil hydraulic conductivity on direct surface runoff hydrographs. *Catena*, *207*, 105693. https://doi.org/10.1016/j.catena.2021.105693

Eck, B. J., Barrett, M. E., & Charbeneau, R. J. (2012). Forchheimer flow in gently sloping layers: Application to drainage of porous asphalt. *Water Resources Research*, *48*(1), W01530. https://doi.org/10.1029/2011WR010837

Eismann, R., & Adams, R. (2018). An explicit and continuous friction factor correlation for helical tubes with arbitrary roughness. *Frontiers in Heat and Mass Transfer*, *11*(4). https://doi.org/10.5098/hmt.11.4

Ellafi, M. A., Deeks, L. K., & Simmons, R. W. (2021). Application of artificial neutral networks to the design of subsurface drainage systems in Libyan agricultural projects. *Journal of Hydrology: Regional Studies*, *35*, 100832. https://doi.org/10.1016/j.ejrh.2021.100832

Forchheimer, P. (1901). Wasserbewegung durch Boden. *Zeitschrift des Verbundes der deutschen Ingenieurs*, *45*, 1782–1788.

FprEN 12697-19:2019 E. (2019). *Bituminous mixtures—Test methods—Part 19: Permeability of specimen*. (Vol. 23, p. B-1040). CEN-CENELEC Management Centre: Rue de la Science.

Govedarica, O., Aškrabić, M., Hadnađev-Kostić, M., Vulić, T., Lekić, B., Rajaković-Ognjanović, V., & Zakić, D. (2022). Evaluation of solidified wastewater treatment sludge as a potential SCM in pervious concrete pavements. *Materials*, *15*(14), 4919. https://doi.org/10.3390/ma15144919

Hammes, G., Thives, L. P., & Ghisi, E. (2018). Application of stormwater collected from porous asphalt pavements for non-potable uses in buildings. *Journal of Environmental Management*, *222*, 338–347. https://doi.org/10.1016/j.jenvman.2018.05.094

Hassanizadeh, S. M., & Grey, W. G. (1987). High velocity flow in porous media. *Transport in Porous Media*, *2*, 521–531.

Hirsch, C. (2007). *Numerical computation of internal and external flows: The fundamentals of computational fluid dynamics* (2nd ed.). Elsevier Butterworth-Heinemann. ISBN: 9780750665940.

Islam, A., Mailapalli, D. R., & Behera, A. (2017). Evaluation of saturated hydraulic conductivity methods for different land uses. *Indian Journal of Ecology*, *44*(3), 456–466.

ISO/FDIS 17312. (2005). *Soil quality—Determination of hydraulic conductivity of saturated porous materials using a rigid-wall permeameter*. International Organization for Standardization.

ISO/TS 17892-11. (2004). *Geotechnical investigation and testing—Laboratory testing of soil—Part 11: Determination of permeability by constant and falling head*. International Organization for Standardization.

Ivetić, M. (1996). *Računska hidraulika—Tečenje u cevima*. University of Belgrade—Faculty of Civile Engineering.

Klute, A. (1986). *Methods of soil analysis. Part 1. Physical and mineralogical methods*. Soil Science Society of America.

Lancheros, J. C., Pumarejo, C. A., Quintana, J. C., Caselles-Osorio, A., & Casierra-Martínez, H. A. (2017). Solids distribution and hydraulic conductivity in multi-cell horizontal subsurface flow constructed wetlands. *Ecological Engineering*, *107*, 49–55. https://doi.org/10.1016/j.ecoleng.2017.06.055

Ljubičić, R., Vićanović, I., Zindović, B., Kapor, R., & Savić, L. (2020). Image processing for hydraulic jump free-surface detection: Coupled gradient/machine learning model. *Measurement Science and Technology*, *31*(10), 104003. https://doi.org/10.1088/1361-6501/ab8b22

Marjanović, D., Vićanović, I., Ljubičić, R., Zindović, B., & Savić, L. (2019). Detekcija nivoa u laboratorijskim kanalima primenom tehnike obrade slika. *Vodoprivreda*, *51*(300–302), 271–280.

19447973, 2023, 7, Downloaded from https://agupubs.onlinelibrary.wiley.com/doi/10.1029/2022WR034158 by INASP/HINARI - SERBIA, Wiley Online Library on [28/11/2023]. See the Terms and Conditions (https://onlinelibrary.wiley.com/terms-and-conditions) on Wiley Online Library for rules of use; OA articles are governed by the applicable Creative Commons License

Mualem, Y. (1976). A new model for predicting the hydraulic conductivity of unsaturated porous media. *Water Resources Research*, *12*(3), 513–522. https://doi.org/10.1029/WR012i003p00513

Nakayama, Y., & Boucher, R. F. (1998). *Introduction to fluid mechanics*. Butterworth-Heinemann.

NEN5789. (2005). *Soil, unsaturated zone, determination of the saturated hydraulic conductivity [In Dutch]*. Nederlandse Norm.

Nijp, J. J., Metselaar, K., Limpens, J., Gooren, H. P. A., & van der Zee, S. E. A. T. M. (2017). A modification of the constant-head permeameter to measure saturated hydraulic conductivity of highly permeable media. *MethodsX*, *4*, 134–142. https://doi.org/10.1016/j.mex.2017.02.002

Nikuradse, J. (1933). *"Strömungsgesetze in rauhenRohren"*. VDIVerlag.

Nimmo, J. R., & Mello, K. A. (1991). Centrifugal techniques for measuring saturated hydraulic conductivity. *Water Resources Research*, *27*(6), 1263–1269. https://doi.org/10.1029/91WR00367

Pedescoll, A., Uggetti, E., Llorens, E., Granés, F., García, D., & García, J. (2009). Practical method based on saturated hydraulic conductivity used to assess clogging in subsurface flow constructed wetlands. *Ecological Engineering*, *35*(8), 1216–1224. https://doi.org/10.1016/j.ecoleng.2009.03.016

Peng, Z., Smith, C., & Stovin, V. (2020). The importance of unsaturated hydraulic conductivity measurements for green roof detention modelling. *Journal of Hydrology*, *590*, 125273. https://doi.org/10.1016/j.jhydrol.2020.125273

Randelovic, A., Zhang, K., Jacimovic, N., McCarthy, D., & Deletic, A. (2016). Stormwater biofilter treatment model (MPiRe) for selected micro-pollutants. *Water Research*, *89*, 180–191. https://doi.org/10.1016/j.watres.2015.11.046

Reynolds, W. D., Bowman, B. T., Brunke, R. R., Drury, C. F., & Tan, C. S. (2000). Comparison of tension infiltrometer, pressure infiltrometer, and soil core estimates of saturated hydraulic conductivity. *Soil Science Society of America Journal*, *64*(2), 478–484. https://doi.org/10.2136/sssaj2000.642478x

Reynolds, W. D., & Elrick, D. E. (1991). Determination of hydraulic conductivity using a tension infiltrometer. *Soil Science Society of America Journal*, *55*(3), 633–639. https://doi.org/10.2136/sssaj1991.03615995005500030001x

Reynolds, W. D., Elrick, D. E., Youngs, E. G., & Amoozegar, A. (2002). Saturated and field saturated water flow parameters. In J. H. Dane & G. C. Topp (Eds.), *Methods of soil analysis. Part 4. Physical methods* (pp. 797–878). SSSA Inc. Publishing.

Richards, L. A. (1931). Capillary conduction of liquids through porous media. *Physics*, *1*(5), 318–333. https://doi.org/10.1063/1.1745010

Sambito, M., Severino, A., Freni, G., & Neduzha, L. A. (2021). Systematic review of the hydrological, environmental and durability performance of permeable pavement systems. *Sustainability*, *13*(8), 4509. https://doi.org/10.3390/su13084509

Sandoval, G. F. B., Galobardes, I., Teixeira, R. S., & Toralles, B. M. (2017). Comparison between the falling head and the constant head permeability tests to assess the permeability coefficient of sustainable Pervious Concretes. *Case Studies in Construction Materials*, *7*, 317–328. https://doi.org/10.1016/j.cscm.2017.09.001

Saxton, K. E., & Rawls, W. J. (2006). Soil water characteristic estimates by texture and organic matter for hydrologic solutions. *Soil Science Society of America Journal*, *70*(5), 1569–1578. https://doi.org/10.2136/sssaj2005.0117

Sheikh, V., van Loon, E., Hessel, R., & Jetten, V. (2010). Sensitivity of LISEM predicted catchment discharge to initial soil moisture content of soil profile. *Journal of Hydrology*, *393*(3–4), 174–185. https://doi.org/10.1016/j.jhydrol.2010.08.016

Smith, W. N., Reynolds, W. D., De Jong, R., Clemente, R. S., & Topp, E. (1995). Water flow through intact soil columns: Measurement and simulation using LEACHM. *Journal of Environmental Quality*, *24*(5), 874–881. https://doi.org/10.2134/jeq1995.00472425002400050013x

Stanić, F., Govedarica, O., Jaćimović, N., Lekić, B., & Ranđelović, A. (2023a). Datasets and Supporting Information for "A novel semi-analytical (inertial) solution for determining permeability of highly pervious porous materials using the two-reservoir laboratory setup" [Dataset]. Zenodo. https://doi.org/10.5281/zenodo.7791905

Stanić, F., Govedarica, O., Jaćimović, N., Lekić, B., & Ranđelović, A. (2023b). Updated Matlab code for "A novel semi-analytical (inertial) solution for determining permeability of highly pervious porous materials using the two-reservoir laboratory setup" [Software]. Zenodo. https://doi.org/10.5281/zenodo.7981417

Stanić, F., Jaćimović, N., Ranđelović, A., & Despotović, J. (2017). Laboratory investigation of hydraulic characteristics of fly ash as a fill material from the aspects of pollutant transport. *Water Science and Technology*, *76*(4), 976–982. https://doi.org/10.2166/wst.2017.243

van Dam, J. C., Huygen, J., Wesseling, J. G., Feddes, R. A., Kabat, P., van Walsum, P. E. V., et al. (1997). *Theory of SWAP. Version 2.0. Simulation of water flow. Solute transport and plant growth in the soil-water-atmosphere-plant environment*. Tech. Publ. 45. Wageningen Agric.

Winston, R. J., Arend, K., Dorsey, J. D., & Hunt, W. F. (2020). Water quality performance of a permeable pavement and stormwater harvesting treatment train stormwater control measure. *Blue-Green Systems*, *2*(1), 91–111. https://doi.org/10.2166/bgs.2020.914

Zeng, Z., & Grigg, R. (2006). A criterion for non-Darcy flow in porous media. *Transport in Porous Media*, *63*(1), 57–66. https://doi.org/10.1007/s11242-005-2720-3

Zhuang, C., Yabing, L., Zhou, Z., Illman, W. A., Dou, Z., Yang, Y., & Wang, J. (2022). Effects of exponentially decaying aquitard hydraulic conductivity on well hydraulics and fractions of groundwater withdrawal in a leaky aquifer system. *Journal of Hydrology*, *607*, 127439. https://doi.org/10.1016/j.jhydrol.2022.127439

19447973, 2023, 7, Downloaded from https://agupubs.onlinelibrary.wiley.com/doi/10.1029/2022WR034158 by INASP/HINARI - SERBIA, Wiley Online Library on [28/11/2023]. See the Terms and Conditions (https://onlinelibrary.wiley.com/terms-and-conditions) on Wiley Online Library for rules of use; OA articles are governed by the applicable Creative Commons License